Article

Cell Reports

The YEATS Domain Histone Crotonylation Readers Control Virulence-Related Biology of a Major Human Pathogen

Graphical Abstract

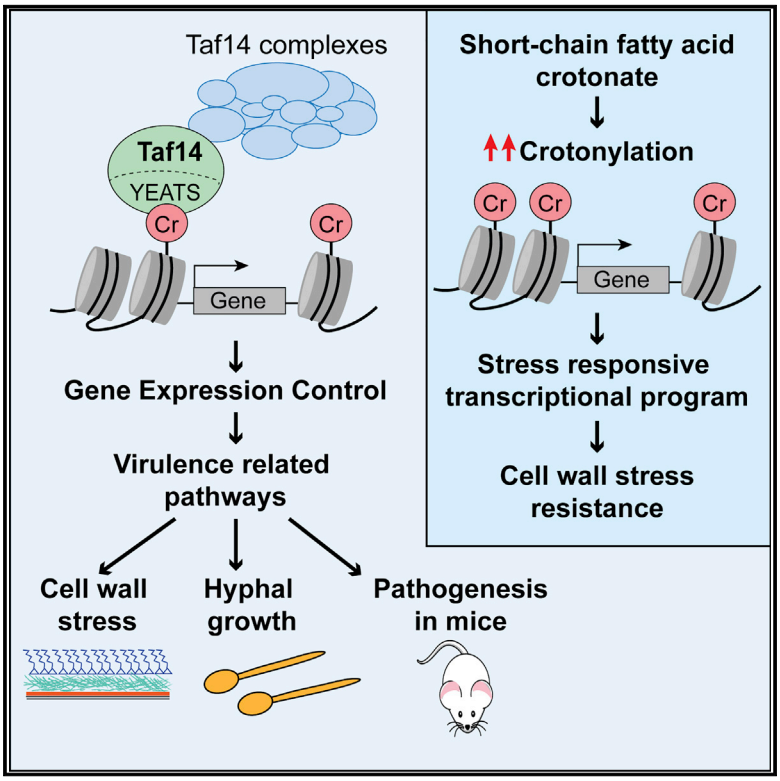

Authors

Qi Wang, Jiyoti Verma, Nikolina Vidan, ..., Mary Sopta, Traude H. Beilharz, Ana Traven

Correspondence

ana.traven@monash.edu

In Brief

Diverse histone acylations expand functional linkages among metabolism, gene regulation, and cellular responses. Wang et al. report that metabolic and stress cues dynamically control histone crotonylation in the human commensal and pathogen *Candida albicans* and show the requirement for crotonylation readers in pathogenesis-related pathways and mammalian virulence.

Highlights

- Metabolism and stress responses control histone crotonylation in *Candida albicans*
- The YEATS crotonylation readers Taf14 and Yaf9 are important for *Candida* virulence
- Taf14 participates in stress responses, cell wall, and filamentation pathways
- The SCFA crotonate affects transcription and stress susceptibility in *Candida*

Wang et al., 2020, Cell Reports *31*, 107528
April 21, 2020
https://doi.org/10.1016/j.celrep.2020.107528

CellPress

Cell Reports
Article

The YEATS Domain Histone Crotonylation Readers Control Virulence-Related Biology of a Major Human Pathogen

Qi Wang,[1,6] Jiyoti Verma,[1,6] Nikolina Vidan,[1,2] Yanan Wang,[1] Timothy M. Tucey,[1] Tricia L. Lo,[1] Paul F. Harrison,[3] Michael See,[3] Angavai Swaminathan,[4] Karl Kuchler,[5] Michael Tscherner,[5] Jiangning Song,[1] David R. Powell,[3] Mary Sopta,[2] Traude H. Beilharz,[4] and Ana Traven[1,7,*]

[1]Infection and Immunity Program and the Department of Biochemistry and Molecular Biology, Biomedicine Discovery Institute, Monash University, Clayton 3800 VIC, Australia
[2]Department of Molecular Biology, Rudjer Boskovic Institute, Bijenicka 54, 10000 Zagreb, Croatia
[3]Bioinformatics Platform, Monash University, Clayton 3800 VIC, Australia
[4]Development and Stem Cells Program and the Department of Biochemistry and Molecular Biology, Biomedicine Discovery Institute, Monash University, Clayton 3800 VIC, Australia
[5]Medical University of Vienna, Center for Medical Biochemistry, Max Perutz Labs, Campus Vienna Biocenter, Dr. Bohr-Gasse 9/2, Vienna, Austria
[6]These authors contributed equally
[7]Lead Contact
*Correspondence: ana.traven@monash.edu
https://doi.org/10.1016/j.celrep.2020.107528

SUMMARY

Identification of multiple histone acylations diversifies transcriptional control by metabolism, but their functions are incompletely defined. Here we report evidence of histone crotonylation in the human fungal pathogen *Candida albicans*. We define the enzymes that regulate crotonylation and show its dynamic control by environmental signals: carbon sources, the short-chain fatty acids butyrate and crotonate, and cell wall stress. Crotonate regulates stress-responsive transcription and rescues *C. albicans* from cell wall stress, indicating broad impact on cell biology. The YEATS domain crotonylation readers Taf14 and Yaf9 are required for *C. albicans* virulence, and Taf14 controls gene expression, stress resistance, and invasive growth via its chromatin reader function. Blocking the Taf14 C terminus with a tag reduced virulence, suggesting that inhibiting Taf14 interactions with chromatin regulators impairs function. Our findings shed light on the regulation of histone crotonylation and the functions of the YEATS proteins in eukaryotic pathogen biology and fungal infections.

INTRODUCTION

Metabolites serve as donors for chromatin modifications and control the activity of chromatin-modifying enzymes (Dutta et al., 2016; Li et al., 2018a). This enables metabolic inputs into chromatin structure, gene expression and, ultimately, regulation of cell biology. A case in point is the regulation of histone lysine acetylation, a mark that drives transcriptional activation. The central intermediate of carbon metabolism, acetyl-CoA, is the donor for histone acetyltransferases (HATs), while the sirtuin histone deacetylases (HDACs) use nicotinamide adenine dinucleotide (NAD^+) as a co-factor, with NAD^+ levels reflecting cellular energetics (Li et al., 2018a).

Mass spectrometry has revealed that the lysine side chains in histone tails can be modified by multiple acyl groups, including crotonyl, succinyl, β-hydroxybutyryl, and propionyl (Chen et al., 2007; Dai et al., 2014; Tan et al., 2011; Xie et al., 2012, 2016). It has been proposed, and there is now evidence, that the acylation status of chromatin is determined by the relative intracellular levels of the acyl-CoA donors (Fellows et al., 2018; Sabari et al., 2015; Simithy et al., 2017). These are derived from metabolic pathways and produced or regulated by microbiota-derived metabolites, such as the short-chain fatty acids butyrate and crotonate. Changing the acylation status of chromatin (more or less acetylated, more or less crotonylated, and so on) greatly diversifies the opportunities to control gene expression by metabolism. Although histone acetylation is vastly more abundant than other acylations (Simithy et al., 2017), the non-acetyl acylations likely play specific functions in cellular responses (Gowans et al., 2019; Sabari et al., 2015; Simithy et al., 2017; Tan et al., 2011; Xie et al., 2016). Indeed, the various acyl groups impart distinct biophysical and chemical properties to chromatin. For example, the crotonyl group, the topic of our study, is more rigid and hydrophobic than acetyl and activates transcription more potently (Sabari et al., 2015). Lysine acylations can also selectively interact with reader proteins, which bind to acyl-lysines to translate histone marks into biological outputs. For instance, bromodomains have preference for acetyl-lysine (Flynn et al., 2015), whereas crotonyl-lysine is bound by the YEATS domain, though not exclusively but with selectivity (Andrews et al., 2016a; Klein et al., 2018; Li et al., 2016; Zhao et al., 2016). The double PHD finger domain (DPF) is another crotonyl-lysine reader (Xiong et al., 2016). The mammalian DBP domain, however, is not conserved in yeast, while the YEATS readers are found throughout eukaryotes as subunits of chromatin-modifying

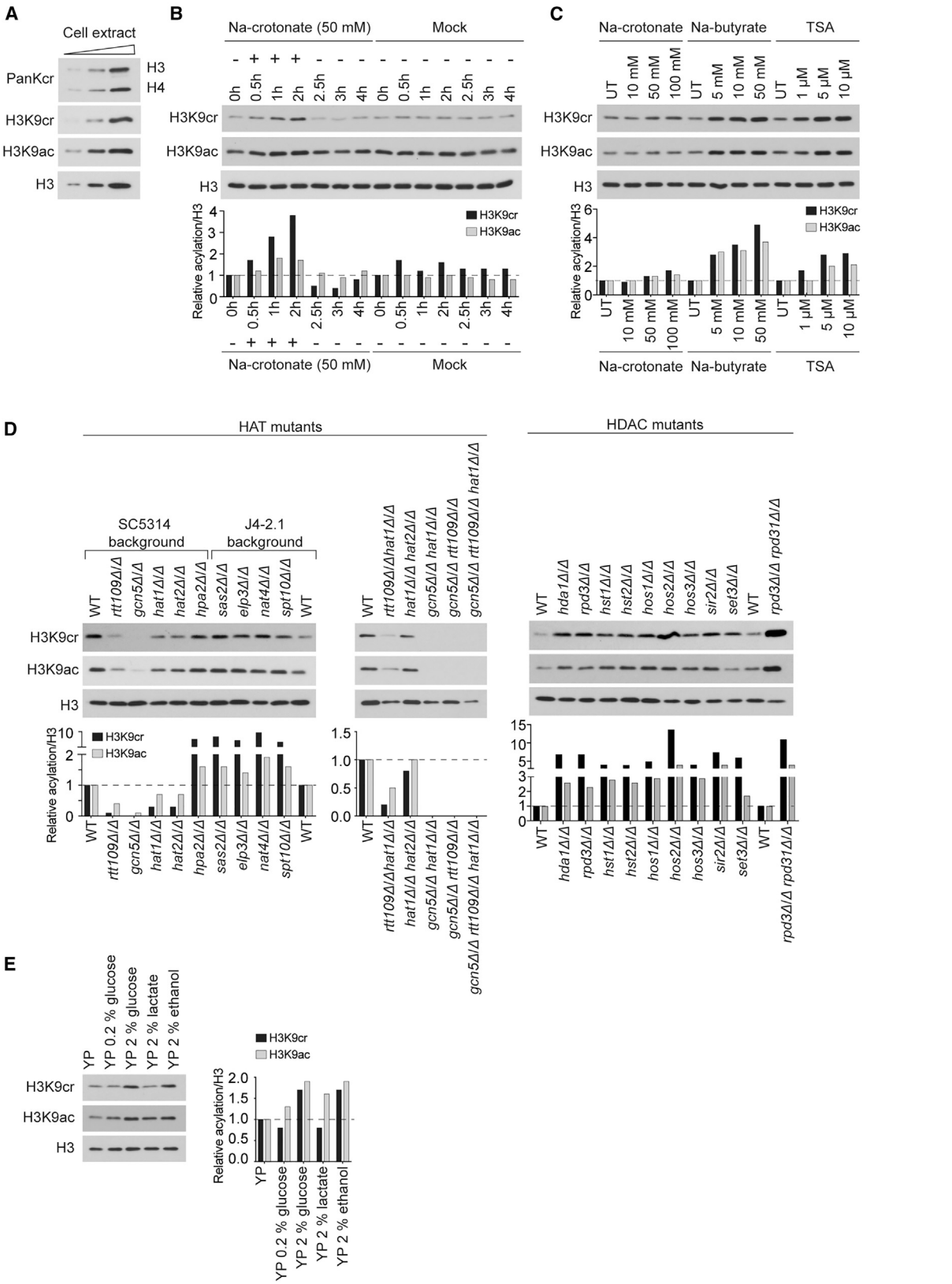

(legend on next page)

complexes (Schulze et al., 2009). The *S. cerevisiae* YEATS protein Taf14 is additionally a subunit of the general transcription factors TFIIF and TFIID (Schulze et al., 2009). The YEATS proteins are thought to "interpret" diverse acylation marks (chiefly crotonylation but also acetylation) in the processes of transcription and DNA repair (Andrews et al., 2016a; Li et al., 2016; Shanle et al., 2015; Zhao et al., 2017).

A major challenge now is to understand how diverse acylations and their readers control cell biology. These processes have been studied in very few species or physiological scenarios (Sabari et al., 2015; Tan et al., 2011; Xie et al., 2016). We reasoned that eukaryotic human microbiota, such as the yeast *Candida albicans*, might be a useful system for this question. As a gut commensal, *C. albicans* is exposed to bacterial metabolites, including short-chain fatty acids that can affect lysine acylations of histones and also other proteins. Moreover, regulatory pathways in *C. albicans* need to be highly responsive to metabolism (Brown et al., 2014). For example, when *C. albicans* switches from commensal to pathogenic colonization, it transitions between metabolically distinct environments of the gut, blood, and internal organs. Metabolic mechanisms determine *C. albicans*-immune interactions (Ballou et al., 2016; Lorenz et al., 2004; Tucey et al., 2018) and drive the cell biology that dictates commensal and virulent states, including gut colonization, biofilm formation, cell wall structure, and the morphological switch from yeast to hyphal cells (Ene et al., 2012; Grahl et al., 2015; Koch et al., 2018; Lindsay et al., 2014; Morales et al., 2013; Pérez et al., 2013; Pradhan et al., 2018; Silao et al., 2019; Verma-Gaur et al., 2015). Despite these considerations, the nexus between metabolism and chromatin remains understudied in this human commensal and pathogen.

Here we characterized the dynamic control of histone crotonylation in *C. albicans* and show that the short-chain fatty acid crotonate broadly affects its gene expression and stress responses. We establish that the YEATS crotonylation readers are required for full virulence of *C. albicans* in a murine model and provide a detailed characterization of Taf14 functions in virulence-related cell biology. Our study sheds lights on a new functional aspect of diverse lysine acylations and their readers in eukaryotes specifically with respect to fungal infections and pathogen biology.

RESULTS

Dynamic Regulation of Histone Crotonylation in *C. albicans*

The presence of histone lysine crotonylation in *C. albicans* chromatin was investigated by immunoblotting using the anti-pan-crotonyllysine and anti-H3K9cr antibodies. These antibodies have been used previously (Andrews et al., 2016a; Sabari et al., 2015), and we confirmed the selectivity of the anti-H3K9cr antibody for crotonylated over acetylated or butyrylated H3K9 peptides (Figure S1A). Crotonylation was observed on histones H3 and H4 (Figures 1A and S1B) and also specifically on H3K9 (Figure 1A). Several non-histone proteins are also crotonylated (Figure S1B). The availability of crotonyl-CoA can be increased by adding sodium crotonate to the medium, resulting in increased histone crotonylation (Sabari et al., 2015). Crotonate caused elevated levels of H3K9cr, and this was reversed by its removal, showing a highly dynamic nature of this mark in *C. albicans* (Figure 1B). Relative to H3K9cr, the effect of crotonate on acetylation of H3K9 (H3K9ac) was less pronounced (Figures 1B and 1C). This is consistent with work indicating that crotonate has relatively smaller activity as an inhibitor of HDACs compared with the related butyrate (Sabari et al., 2015). The levels of H3K9cr in *C. albicans* were sensitive to butyrate (a pan-HDAC inhibitor that can be produced by gut microbiota) (Figure 1C). Another pan-HDAC inhibitor, trichostatin A (TSA), was used in these experiments as a control, and it also increased the levels of H3K9cr and H3K9ac (Figure 1C). Analysis of HAT mutants showed that H3K9cr was highly reduced in *gcn5Δ/Δ* extracts and also largely reduced in *rtt109Δ/Δ*, *hat1-Δ/Δ*, and *hat2Δ/Δ* (Figure 1D). Several HDAC mutants displayed somewhat increased levels of H3K9cr, with the strongest increase seen in the double *rpd3Δ/Δ rpd31Δ/Δ* strain (Figure 1D). Finally, the relative levels of H3K9cr changed depending on the nature and concentration of carbon source. Compared with

Figure 1. Lysine Crotonylation Is a Dynamic Histone Modification in *C. albicans*

(A) Western blot analysis of increasing amounts of whole-cell extract isolated from log phase cultures grown in rich medium (YPD, 2% glucose). Individual gels (×4) were loaded with identical whole-cell extracts, and western blots performed with antibodies to detect total lysine crotonylation (Pan-Kcr), H3K9cr, H3K9ac, and total H3, respectively.

(B) Na-crotonate (50 mM) was added to log phase YPD-grown yeast cultures and samples taken at the indicated time points (indicated by +). For crotonate removal, cells were centrifuged, washed, and resuspended in YPD medium without crotonate (indicated by − and staring at the 2.5 h time point). Individual gels (x3) were loaded with identical whole-cell extracts and western blots performed as in (A) using antibodies against H3K9cr, H3K9ac, or total H3, respectively. Bar graph shows quantification of H3K9cr or H3K9ac levels normalized to total H3, in the presence or absence of Na-crotonate. Normalized H3K9cr or H3K9ac levels at 0 h in Na-crotonate samples were set to 1, and values for the other time points calculated relative to that.

(C) Western blots were performed as in (B) but in the presence of increasing doses of Na-crotonate, Na-butyrate, or TSA treatment for 2 h. Bar graph shows quantification of the levels of H3K9cr or H3K9ac normalized to total H3. Untreated (UT) control sample of each treatment was set to 1 and other values calculated relative to that.

(D) Western blots to detect H3K9cr were performed as in (B), using whole-cell extracts from HATs and HDACs mutants of *C. albicans*. H3K9ac and total H3 are shown as controls. Bar graph shows quantification of the levels of H3K9cr or H3K9ac normalized to H3. Each set of strains was compared with its wild-type (WT) control (SC5314 or J4-2.1) set to 1, and all other values were calculated relative to that. For HDAC western blots, single mutants were compared with the WT control on the left side (lane 1) of the membrane, and the double *rpd3Δ/Δ rpd31Δ/Δ* mutant was compared with the adjacent WT control (lane 11) on the right side of the membrane.

(E) Log phase, YPD-grown cultures were transferred to the indicated medium and grown for 3 h, followed by preparation of whole-cell extracts and western blots as in (B). Bar graph shows quantification of the levels of H3K9cr or H3K9ac normalized to H3. The YP sample was set to 1, and all other values were calculated relative to that.

For all panels, Ponceau-stained membranes are shown in Figure S1 to demonstrate equal loading. Uncropped western blots are shown in Figure S6. Independent biological repeats for the experiments are shown in Figure S7.

standard yeast growth conditions (2% glucose), the relative levels of H3K9cr were reduced in 0.2% glucose and 2% lactate, but unchanged in 2% ethanol (Figure 1E). The levels of H3K9ac were for the most part co-regulated with H3K9cr (Figure 1E). These data suggest that H3K9cr responds to cellular metabolism in *C. albicans*.

The YEATS Crotonyl-Lysine Readers Are Conserved in Fungi and Control *C. albicans* Virulence

Bioinformatics analyses using a hidden Markov model revealed that 316 of 319 fungal species analyzed encode YEATS crotonyl-lysine readers in their genome (Figure 2A; Data S1). Most of the common human fungal pathogens have two YEATS proteins, with the exception of *C. glabrata* (which has three) and *Cryptococcus* (which has one) (Figure 2B). The two *C. albicans* YEATS proteins are homologous to *S. cerevisiae* Taf14 (encoded by C2_04220C) and Yaf9 (encoded by C7_03770C). *C. albicans* Yaf9 is a subunit of the chromatin regulators SWR1 and NuA4 with roles in hyphal morphogenesis (Wang et al., 2018). This is similar to *S. cerevisiae* and shows that, as in other eukaryotes, the *C. albicans* YEATS proteins have roles in chromatin regulation. The cellular roles of the *C. albicans* YEATS proteins remain poorly characterized. Thus, we constructed homozygous deletion mutants of *YAF9* or *TAF14* (Figure S2A). Both mutants displayed slow growth in rich glucose medium at 30°C, with *yaf9Δ/Δ* having a stronger defect (Figures 2C and 2D). The *yaf9-Δ/Δ* mutant grew very slowly at human body temperature of 37°C and was unable to grow at 42°C (Figure 2C). Both mutants grew on non-fermentative carbon sources lactate, glycerol, and ethanol at 30°C, but less so at higher temperatures (Figure 2C). These growth phenotypes were rescued by reintroducing wild-type *TAF14* or *YAF9* genes into the respective mutants (Figures 2C and 2D). Deletion of *TAF14* led to haploinsufficient phenotypes. The heterozygous mutant and the deletion mutant complemented with one copy of the *TAF14* gene displayed lower *TAF14* expression and partially defective phenotypes (Figures S2B–S2D). Introduction of a second copy of *TAF14* into the mutant resulted in wild-type levels of *TAF14* expression and full complementation of phenotypes (Figures 2B- S2D).

Consistent with important roles for the *C. albicans* YEATS proteins in host environments, both *taf14Δ/Δ* and *yaf9Δ/Δ* showed attenuated virulence in the murine bloodstream infection model (Figure 2E) and displayed reduced fungal burden in kidneys (Figure 2F). The virulence defects were either fully (for *taf14Δ/Δ*) or partially (for *yaf9Δ/Δ*) complemented in the reconstituted strains (Figures 2E and 2F).

Taf14 Mediates Stress Responses and Controls an Adaptive Transcriptional Program

For the remaining work, we focused on Taf14 to dissect its cellular roles in detail. First, we tested the susceptibility of *taf14-Δ/Δ* to stressors important for *C. albicans* in host niches, such as cell membrane and cell wall stress as well as oxidative and osmotic stress. The mutant was susceptible to DMSO, formamide, and osmotic stress (NaCl), but did not appear susceptible to SDS or oxidative stress (Figure 3A). These phenotypes were consistent with three independent deletion clones (Figure S2E) and were complemented in the reconstituted strain (Figure 3A). Strikingly, *taf14Δ/Δ* cells displayed high resistance to cell wall stress induced by calcofluor white (CFW) or Congo red (CR) (Figure 3A) and was moderately resistant to cell wall degradation by zymolyase (Figure 3B). Cell wall stress resistance showed haploinsufficiency (Figure S2C). Consistent with altered cell walls, the *taf14Δ/Δ* mutant displayed heightened activation of cell wall stress signaling, as judged by higher levels of phosphorylated Mkc1 and Cek1 kinases relative to the wild-type (Figure 3C). Further indicative of cell wall changes in the mutant, *taf14Δ/Δ* cultures had elevated levels of pseudohyphae-like cell chains under budding yeast growth conditions (Figures 3D and 3E). The mutant was also defective in hyphal morphogenesis, which requires cell wall remodeling and is a key virulence property of *C. albicans*. This defect was strong on solid media, with very few hyphae protruding from *taf14Δ/Δ* colonies (Figure 3F). Hyphal growth was also partially compromised in the heterozygous mutant (Figure S2D). In liquid media, the *taf14Δ/Δ* mutant formed hyphae with shorter filaments compared to the wild-type (Figures 3G and 3H).

Next, we used RNA sequencing (RNA-seq) to uncover the transcriptional program regulated by *C. albicans* Taf14. We compared *taf14Δ/Δ* with the wild-type during standard log phase growth and in response to CFW-induced cell wall stress. Treatment with 20 μg/mL CFW for 2 h stopped growth of the wild-type and activated stress-responsive genes without causing evident cell death (Figure S3). Thus, this condition was used for transcriptional profiling. All differentially expressed genes are shown in Data S2, and the complete data can be viewed interactively at http://rnasystems.erc.monash.edu/2019/verma_et-al/. Inspection of the RNA-seq data did not detect evidence of larger chromosomal changes or aneuploidies in the mutant (Figure S4).

During log phase growth without stress, *taf14Δ/Δ* cells differentially expressed some 1,245 genes (cutoff of $\log_2 = 1$ and false discovery rate [FDR] ≤ 0.01) (Data S2). Approximately half of the differentially expressed genes were upregulated in the mutant, and half were downregulated. Gene Ontology (GO) analysis revealed that genes upregulated in *taf14Δ/Δ* cells include those with functions in ncRNA processing and metabolism (including tRNA, rRNA, and snRNA), ribosome biogenesis, and nucleic acid metabolism (Data S2). Downregulated genes include functional classes involved in various metabolic processes, including carbohydrate metabolism and oxidation-reduction (Data S2). Approximately 5% of up- and downregulated genes in *taf14Δ/Δ* cells encode cell wall components (Data S2).

Strikingly, the transcriptional profile of the *taf14Δ/Δ* mutant without stress resembled CFW-treated wild-type (Figure 4A). There was a ~70% (67.488) overlap in differentially expressed genes (Figure 4B), and similar functional categories were affected in both conditions (Data S2). Although the GO term was not significantly enriched, many cell wall genes were differentially expressed in CFW-treated wild-type (Figure 4C; Data S2). Detailed analysis showed that genes of chitin and glucan synthesis and remodeling were upregulated by cell wall stress, and the same sets were upregulated in *taf14Δ/Δ* without stress (Figure 4C; Data S2). The mutant downregulated genes encoding wall degrading enzymes such as the chitinase *CHT3* and the glucanase *ENG1* (Figure 4C; Data S2), which is consistent with

A

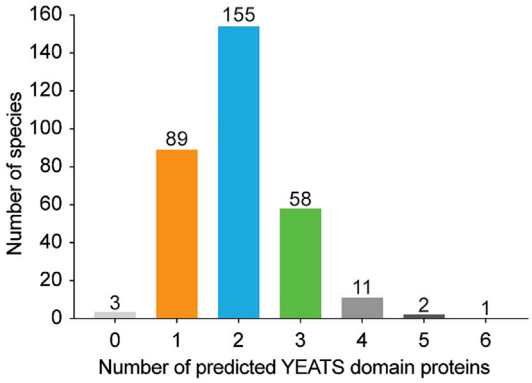

B

Strains	Number of YEATS proteins	Types of YEATS proteins
Sacchromyces cerevisiae	3	Yaf9, Taf14, Sas5
Candida albicans	2	Yaf9, Taf14
Candida glabrata	3	Yaf9, Taf14, Sas5
Aspergillus fumigatus	2	Yaf9, Taf14
Cryptococcus neoformans	1	Yaf9
Histoplasma capsulatum	2	Yaf9, Taf14
Paracoccidioides brasiliens	2	Yaf9, Taf14
Talaromyces marneffei	2	Yaf9, Taf14

C

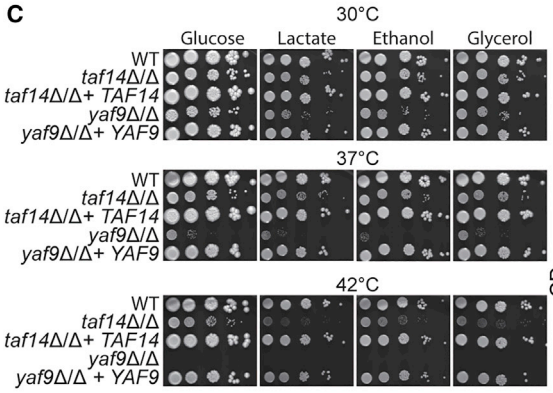

D

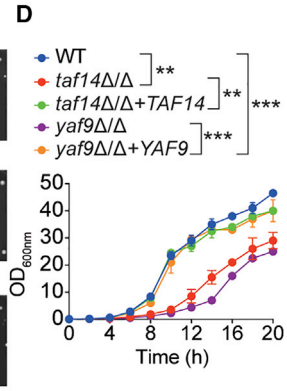

E

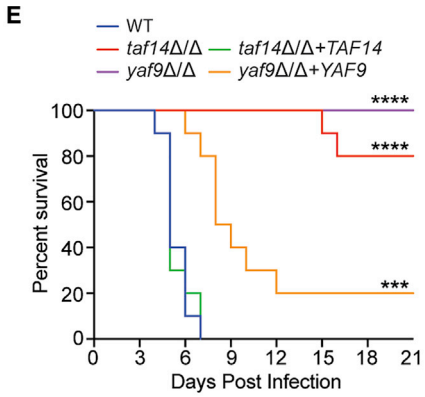

F

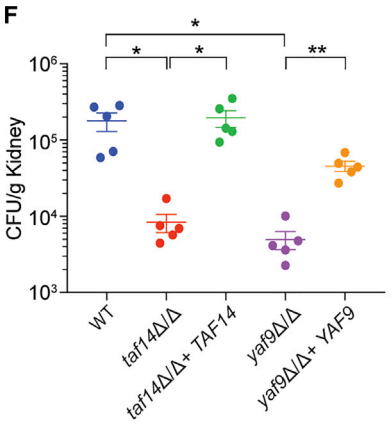

Figure 2. The YEATS Readers Are Widely Conserved in Fungi and Required for Fitness and Virulence of *C. albicans*

(A) Distribution of YEATS proteins in fungal species. Shown is the number of YEATS proteins in the fungal species analyzed. See Data S1 for details.

(B) Distribution of YEATS proteins in the indicated human fungal pathogens and their homology to Yaf9, Taf14, and Sas5 from *S. cerevisiae*.

(C) *C. albicans* WT, YEATS mutants and complemented strains were grown on YP (yeast extract, peptone) with glucose, lactate, glycerol, or ethanol as the carbon source (all at 2%). Plates were incubated for 3 days at 30°C, 37°C, or 42°C. The *taf14*-complemented strain has two copies of *TAF14*, while the *yaf9*-complemented strain has one copy of *YAF9*.

(D) Growth curves of indicated strains grown in YPD at 30°C. Overnight cultures were diluted to OD_{600} = 0.1, and OD values were measured every 2 h. Shown are the averages ± SEM from two independent experiments. Statistical analysis of the indicated strains at the 12 h time point is shown. **p < 0.01 and ***p < 0.001 (one-way ANOVA followed by Tukey's multiple-comparisons test).

(E) The murine tail vein model of candidaemia was used, with an infectious load of *C. albicans* of 3 × 10^5 colony-forming units. Animal survival over time is shown (n = 10 mice/group). ***p < 0.001 and ****p < 0.0001 (Mantel-Cox test).

(F) Fungal load in kidneys was determined at day 3 post-infection (n = 5 mice/group). *p < 0.05 and **p < 0.01 (one-way ANOVA followed by Tukey's multiple-comparisons test). Each data point is from an individual animal; also shown are the mean and the SEM.

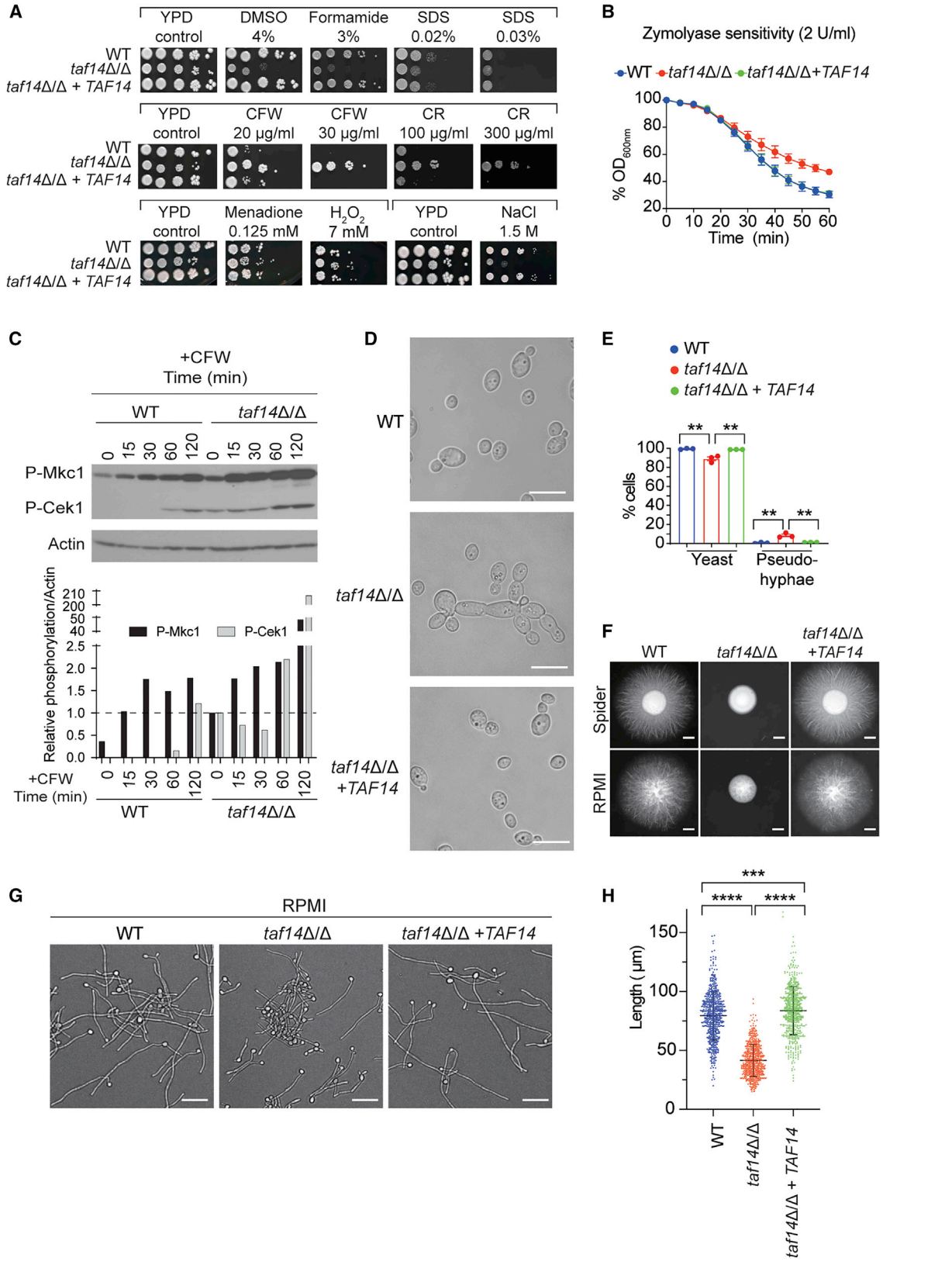

(legend on next page)

increased levels of pseudohyphae-like cell chains (Figures 3D and 3E). Follow-up qPCR experiments showed variable downregulation of these wall degrading enzymes, possibly due to their cell cycle-dependent activation that is not controlled for in asynchronous cultures in our experiments (Côte et al., 2009), and known roles of *S. cerevisiae* Taf14 in cell cycle control (Dahan and Kupiec, 2004).Upregulation of several glucan-related genes in *taf14Δ/Δ* cells was confirmed by qPCR (Figure 5E). Genes encoding cell surface proteins and mannosylation-related functions were also differentially expressed in unstressed *taf14Δ/Δ* and upon cell wall stress in the wild-type (Figure 4C; Data S2).

There were some exceptions to the congruence in cell wall gene regulation in unstressed *taf14Δ/Δ* and stressed wild-type. For example, the mannosyltransferase genes *MNN22* and *MNN15* were strongly repressed in *taf14Δ/Δ* cells but not as much by cell wall stress (Figure 4C). Also, the cell wall adhesin *ALS1* and the chitinase *CHT1* were downregulated in the mutant but activated by cell wall stress in the wild-type (Figure 4C). Thus, Taf14 has roles in cell wall gene expression that are not explained by a constitutively active stress response. Collectively, the transcriptomics data indicate that Taf14 is needed for transcription of genes implicated in cell wall architecture and function. Their altered expression leads to cell wall disruptions that trigger constitutive activation of stress signaling and modifications that fortify the wall, such as increased glucan and chitin. Constitutive activation of stress responses in *taf14Δ/Δ* cells could explain their resistance to CFW and CR (Figure 3A).

The Chromatin Reader Function of Taf14 Drives Cell Wall and Hyphal Morphogenesis Phenotypes

Structures of the *S. cerevisiae* Taf14 YEATS domain have shown that tryptophan 81 (W81) mediates the interaction with crotonylated and acetylated H3K9 and contributes to Kcr recognition via so-called π-π-π stacking (Andrews et al., 2016a; Klein et al., 2018; Shanle et al., 2015). The equivalent residue in *C. albicans* Taf14 is W80. To test the roles of Taf14 chromatin-reader activity in *C. albicans*, we constructed the W80A mutant and studied its phenotypes. The Taf14 W80A protein was expressed at similar levels to the wild-type (Figure S5A), showing that the mutation does not compromise overall protein structure/folding. The *C. albicans* Taf14 interacted robustly with H3K9cr, and the W80A mutation abrogated the interaction (Figure 5A). Compared with H3K9cr, the interaction with H3K9ac peptide was much less pronounced (Figure 5A). This shows selectivity of the *C. albicans* Taf14 YEATS domain for crotonyl-lysine over acetyl-lysine. The H3K9-crotonyl mark read by Taf14 was detected at promoter regions of two selected cell wall and filamentation-related genes, *ALS1* and *HWP1*, in the absence and presence of cell wall stress (Figure 5B). Consistent with YEATS domain functions in cell wall and filamentation, the W80A mutant was resistant to CFW and CR and displayed defective filamentation, with similar though milder phenotypes compared with *taf14Δ/Δ* (Figures 5C and 5D). Moreover, the cell wall genes *ALS1*, *MNN22*, and *ECM331* were downregulated in the W80A mutant (Figure 5E), showing that their expression needs the chromatin reader function of Taf14. The upregulation of *PHR1*, *KRE1*, and *EXG2* seen in *taf14-Δ/Δ* was not recapitulated in W80A cells (Figure 5E), in line with milder cell wall stress phenotypes (Figure 5C). Further data indicate that *C. albicans* Taf14 has functions that are independent of its reader role. The W80A mutant grew better than the null strain under control conditions (without stress), it was not susceptible to DMSO, formamide, or osmotic stress, and appeared resistant to oxidative stress (Figure 5C; see also Figure 6A for growth curves).

Blocking the C-Terminal Domain of Taf14 Cripples Fitness and Virulence of *C. albicans*

We next performed experiments to understand the YEATS-independent roles of *C. albicans* Taf14. *S. cerevisiae* Taf14 uses the N-terminal YEATS domain to interact with acylated histones and the C-terminal domain to interact with the complexes of which it is a subunit (Feigerle and Weil, 2016; Schulze et al., 2010). Unlike the YEATS domain, the C terminus of yeast Taf14 does not bear obvious conservation with human YEATS proteins (Schulze et al., 2009), and it could be interesting for any future antifungal targeting. Initially, we created a mutant in which the entire C terminus of Taf14 was deleted (i.e., only the YEATS domain was present). However, we could not detect expression of the YEATS-only protein in our initial western blot experiment, precluding conclusions about phenotypic data. As an alternative approach, we introduced a TAP tag at the Taf14 C terminus in an attempt to block its function (see STAR Methods for strain construction). TAP-tagged Taf14 was expressed at wild-type levels (Figure S5B), showing that the tag did not compromise

Figure 3. The *taf14Δ/Δ* Mutant Displays Altered Stress Responses and Morphogenesis

(A) Stress susceptibility of the *taf14Δ/Δ* mutant was tested on plates containing the indicated compounds. Plates were incubated at 30°C for 3 days.

(B) Stationary-phase cultures grown in YPD were treated with Zymolyase, and OD_{600} values were measured over time. Data are expressed as percentage absorbance relative to the initial OD_{600} value. Shown are the averages ± SEM from three independent experiments.

(C) Log phase cultures were treated with 20 μg/mL calcofluor white (CFW) and sampled over time, where 0 represents untreated samples collected just before CFW addition. The p44/42 anti-Erk antibody was used to detect the phosphorylated forms of the Mkc1 (P-Mkc1) and Cek1(P-Cek1) kinases. Actin was used as the loading control. Bar graph shows quantification of the levels of P-Mkc1 and P-Cek1 normalized to actin. Untreated *taf14Δ/Δ* was set to 1, and all other values were calculated relative to that. The uncropped western blot is shown in Figure S6F.

(D) Representative cell morphology of the indicated strains grown to stationary phase. Images were taken at 100× magnification. The scale bar is 10 μm.

(E) Quantification of cell morphology (yeast and pseudohyphae) in cell populations. The experiment was repeated three times, with at least 200 cells counted per strain each time. The error bar denotes SEM. **$p < 0.01$ (one-way ANOVA followed by Tukey's multiple-comparisons test).

(F) Hyphal morphology of the indicated strains grown on filamentation-inducing plates (Spider or RPMI). Incubation was for 5 days at 37°C. The scale bar is 1 mm.

(G) Hyphal morphology of indicated strain grown in RPMI medium. Overnight cultures were washed and diluted to $OD_{600} = 0.2$ into RPMI medium. Images were taken after 4.5 h of growth at 37°C (200 rpm) at 40× magnification. The scale bar is 25 μm.

(H) Measurements of hyphal lengths of indicated strains grown in RPMI as in (G). Data are from three independent experiments. In each experiment, 200 cells per strain were measured. The error bar denotes SEM. ***$p < 0.001$ and ****$p < 0.001$ (one-way ANOVA followed by Tukey's multiple-comparisons test).

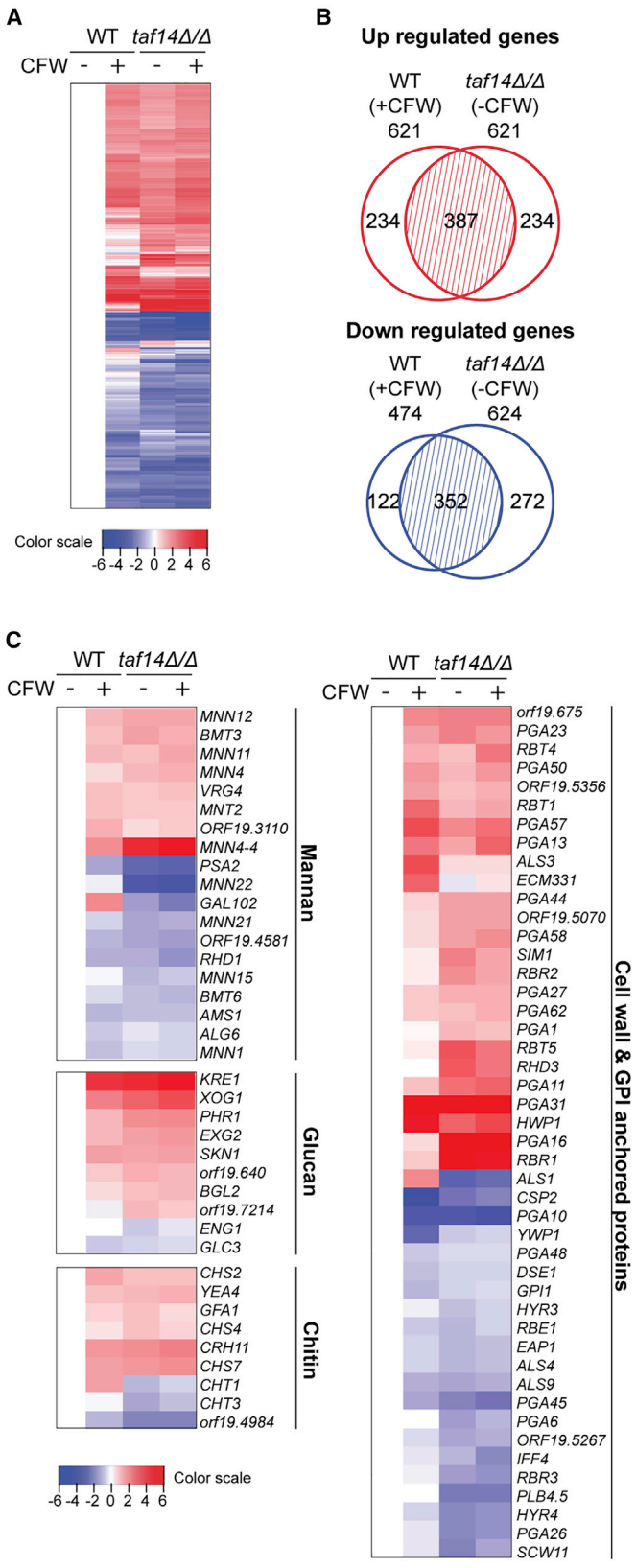

Figure 4. Taf14 Is Needed for Appropriate Regulation of the Cell Wall Stress-Dependent Transcriptional Program

(A) Heatmaps of changes in gene expression of differentially regulated genes in CFW-treated WT, untreated *taf14Δ/Δ* and CFW-treated *taf14Δ/Δ*, all relative to untreated WT (FDR $\leq$ 0.01, $\log_2 = 2$). The entire gene list is in Data S2 and can be interactively viewed at http://rnasystems.erc.monash.edu/2019/verma_et-al/. CFW, calcofluor white.

(B) Venn diagram of genes differentially expressed in CFW-treated WT versus untreated *taf14Δ/Δ* with untreated WT as the baseline for comparison in both cases (FDR < 0.01, $\log_2 = 1$). The gene list used to construct the Venn diagram is shown in Data S2.

(C) Heatmaps of changes in gene expression of cell wall-related genes relative to untreated WT (FDR $\leq$ 0.01 and $\log_2 = 1$ were used as cutoffs to construct the list of genes).

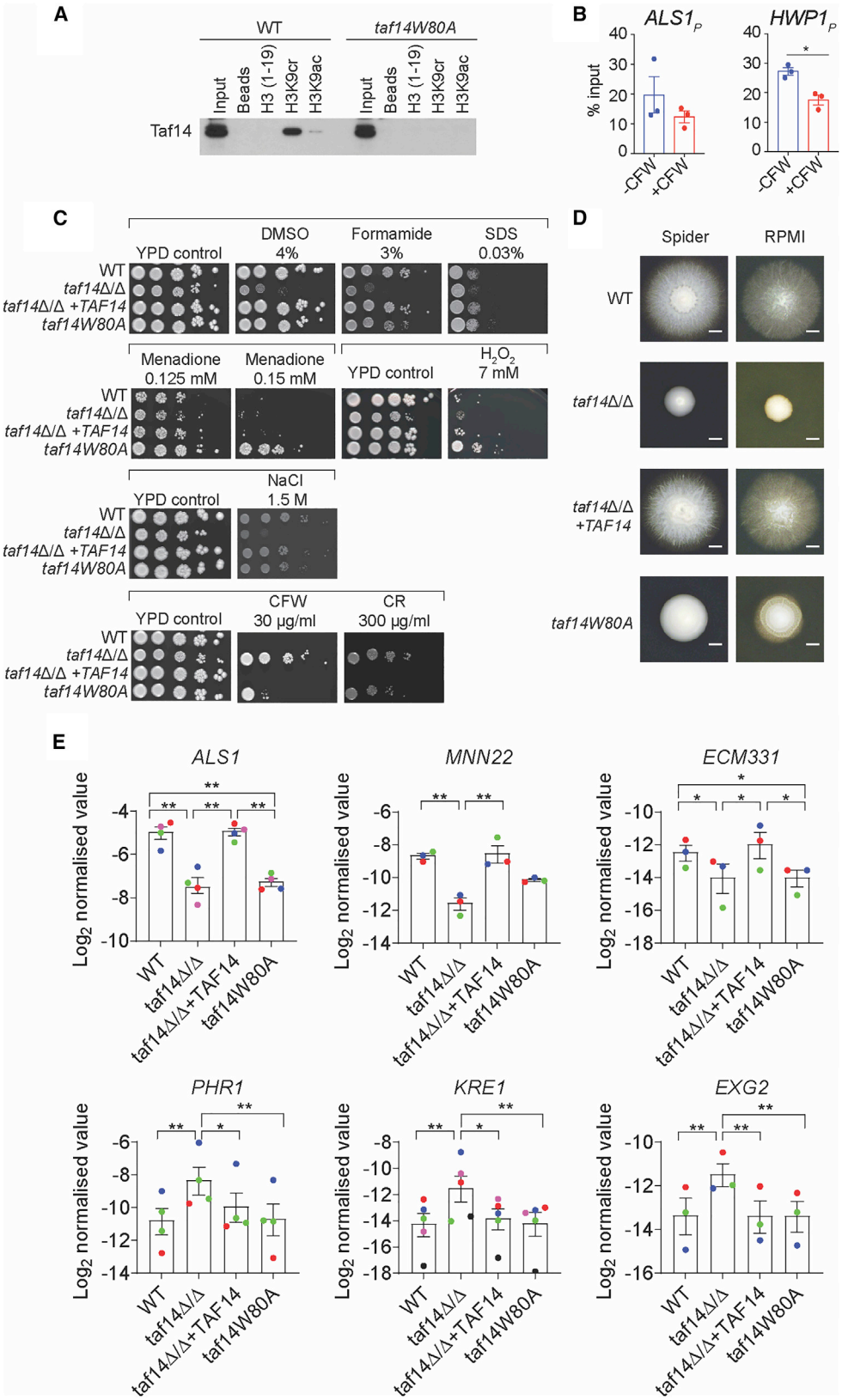

(legend on next page)

Taf14 expression or stability. Nevertheless, the TAP-tagged strain displayed slow growth comparable with *taf14Δ/Δ* (Figure 6A), and it displayed stress phenotypes that were similar to the null strain, including susceptibility to DMSO, formamide, and osmotic stress, and resistance to cell wall stress (Figure 6B). The TAP-tagged strain was also compromised for filamentation, with an intermediate phenotype between the wild-type (which could filament well) and *taf14Δ/Δ* (which was drastically compromised) (Figure 6C). The TAP-tagged strain displayed reduced kidney burden and weight loss in the murine bloodstream infection model that was comparable with the *taf14Δ/Δ* null, while the W80A YEATS domain mutant behaved like the wild-type (Figures 6D and 6E). Thus, blocking the C-terminal domain of Taf14 is critical for reducing virulence of *C. albicans*.

The Short-Chain Fatty Acid Crotonate Triggers Stress-Responsive Transcription and Rescues *C. albicans* from Cell Wall Stress

To further explore the links between histone crotonylation and stress responses in *C. albicans*, we turned to the short-chain fatty acid crotonate, which is converted to crotonyl-CoA, leading to elevated histone crotonylation (Figure 1). H3K9cr levels increased over time upon treatment with CFW (Figure 7A), consistent with a role for histone crotonylation in cell wall stress responses. Intriguingly, crotonate rescued the susceptibility of wild-type *C. albicans* to CFW in a dose-dependent manner (Figure 7B). Addition of NaCl at the same doses had no effect (Figure 7B). This shows that sodium crotonate does not simply cause osmotic stabilization, but it has a specific effect in promoting cell wall stress resistance. The *taf14* W80A mutant was also rescued by crotonate. The mutant was resistant to CFW, but crotonate improved growth (Figure 7B).

RNA-seq showed that crotonate triggers a large transcriptional response in *C. albicans*, and the *taf14Δ/Δ* mutant without treatment resembled crotonate-treated wild-type, with some exceptions (Figure 7C). This recapitulates differential expression of stress-responsive genes in untreated *taf14Δ/Δ* shown in the previous experiment in Figure 4. The changes were overall less pronounced, indicating that the mutant has better adapted over time. Crotonate further activated or repressed gene expression in *taf14Δ/Δ* for many affected genes (Figure 7B).

Interestingly, the crotonate response paralleled the CFW response (Figure 7D). There was a 66.8% overlap of genes induced by crotonate with those induced by CFW and a 57.6% overlap for the repressed genes (Figure 7D). As was the case for CFW-treated cells, GO analysis of upregulated genes in wild-type cells responding to crotonate identified functional categories related to RNA processing and ribosome biogenesis and downregulation of metabolic functions (Data S2). Although genes related to the cell wall were not enriched in the GO analysis, inspection of the transcriptome revealed that crotonate did in fact trigger differential expression of genes required for chitin and glucan synthesis and remodeling, protein mannosylation, and those encoding cell wall proteins (Figure 7E). Regulation of a major stress-induced transcriptional program provides an explanation for crotonate-dependent rescue of *C. albicans* growth under cell wall stress.

DISCUSSION

Here we establish that histone lysine crotonylation is a dynamic chromatin mark in *C. albicans*, which is regulated by stress and metabolic inputs relevant to host immune surveillance. Carbon source scenarios that parallel host conditions, such as changing glucose levels and the presence of lactate, modulate the levels of the H3K9cr mark in *C. albicans* (Figure 1E). Compared with glucose, growth on lactate modulates susceptibility of *C. albicans* to various stresses and changes cell wall structure, promoting hiding from the immune system and virulence in mouse models (Ballou et al., 2016; Ene et al., 2012). Our data now show that a key downstream effect of changing carbon source is regulation of chromatin acylations levels (crotonylation and also acetylation), expanding the opportunities to globally control adaptive gene expression programs by carbon source. The short-chain fatty acids butyrate and crotonate also increase the levels of H3K9cr (Figure 1). These links provide possibilities for cross-microbiome ''talk'' between *C. albicans* and bacteria, as butyrate is abundantly produced by bacterial microbiota in the gut, where *C. albicans* resides as a commensal. There is also evidence that an intestinal bacterium can release crotonyl-CoA, the donor for histone crotonylation (Huang et al., 2018).

The levels of H3K9cr also increase in response to cell wall stress (Figure 7A). Moreover, addition of crotonate to the growth medium increases histone crotonylation and triggers transcriptional reprogramming that parallels CFW-induced cell wall stress. This explains how crotonate rescues *C. albicans* in the presence of CFW by promoting gene expression that might be

Figure 5. The Chromatin Reader Function of Taf14 Is Required for Cell Wall and Hyphal Morphogenesis Phenotypes

(A) Binding of Taf14 to H3K9cr and H3K9ac peptides. Taf14 western blot of peptide pull-down assays were performed using cell lysate from the WT and the strain mutated in the Taf14 YEATS domain (*taf14W80A*). Uncropped western blot is shown in Figure S6G.

(B) qPCR analysis of H3K9cr chromatin immunoprecipitation (ChIP) samples from WT *Candida* cells treated with ± 20 μg/mL calcofluor white (CFW) for 30 min. Primers were designed for promoter regions of the indicated cell wall genes. Data are represented as mean of three biological replicates ± SEM. *$p < 0.05$ (Welch's t test).

(C) Ten-fold serial dilutions of cultures of the indicated strains were spotted on plates with or without stressors and incubated for 3 days at 30°C.

(D) Hyphal morphology of the indicated strains grown on filamentation-inducing plates (Spider and RPMI). Incubation was for 5 days at 37°C. Shown are representative colonies from three independent experiments. The scale bar is 1 mm.

(E) qPCR analysis of indicated genes in WT, *taf14Δ/Δ*, *taf14Δ/Δ+TAF14*, and *taf14W80A*. The reference gene is *RDN5*. The data are presented as $\log_2$-transformed normalized expression values. Data are shown from three, four, or five independent biological experiments, and the error bar denotes SEM. Data from the independent experiments are shown using different colors. In the case of *PHR1*, one of the three independent experiments used cultures from two independent colonies for each of the strains. Statistical analysis was performed on $\log_2$-transformed normalized expression values. Only comparisons shown to be significant are displayed. *$p < 0.05$ and **$p < 0.01$ (two-way ANOVA followed by Tukey's multiple-comparisons test).

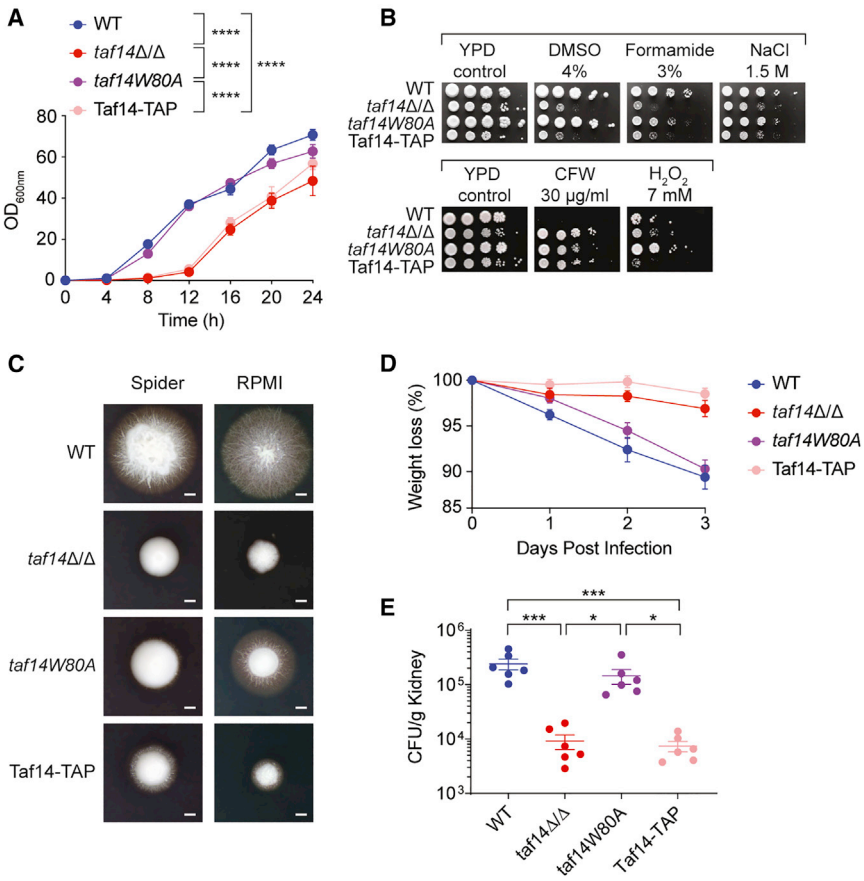

Figure 6. The C-Terminal Domain of Taf14 Drives Fitness and Virulence of *C. albicans*

(A) Growth curves of the indicated mutants grown in YPD at 30°C. Cultures from three independent colonies for each of the strains were assayed together in one experiment. Shown are the averages and SEM from the three cultures. Statistical analysis of the indicated strains at the 12 h time point is shown. ****p < 0.0001 (one-way ANOVA followed by Tukey's multiple-comparisons test).

(B) Ten-fold serial dilutions of cultures of the indicated strains were spotted on plates with or without stressors and incubated for 3 days at 30°C.

(C) Hyphal morphology of the indicated strains grown on filamentation-inducing plates (Spider and RPMI). Incubation was for 5 days at 37°C. The scale bar is 1mm.

(D) Weight loss of mice (n = 6 mice/group) infected via the tail vein with 3 × 10^5 colony-forming units of the indicated *C. albicans* strains. The p values were not significant (one-way ANOVA followed by Tukey's multiple-comparisons test).

(E) Fungal load in kidneys was determined at day 3 post-infection of mice from (D). Each data point is from an individual animal; also shown are the mean and the SEM. *p < 0.05 and ***p < 0.001 (one-way ANOVA followed by Tukey's multiple-comparisons test).

needed for growth under stress. Our data suggest that crotonate and Taf14 act redundantly to regulate cell wall stress responses, as both crotonate and deletion of *TAF14* lead to CFW resistance, the *taf14*W80A reader domain mutant is rescued by crotonate in the presence of CFW, and the *taf14Δ/Δ* strain can respond transcriptionally to crotonate. *S. cerevisiae* data suggest that histone crotonylation acts via Taf14 in growth-dependent transcription (Gowans et al., 2019). Our study now indicates that metabolic and stress context dictate how crotonate, histone crotonylation, and the chromatin readers cooperate. Additionally, crotonate could act via crotonylation of proteins other than histones, as our data show that multiple non-histone proteins are crotonylated in *C. albicans* (Figure S1B). Crotonate could also trigger metabolic remodeling beneficial to surviving stress, which is an exciting area to explore in the future.

Our data define the enzymes that control histone crotonylation in *C. albicans*. The H3K9cr mark is regulated mainly by the HAT Gcn5. Rtt109, Hat1, and Hat2 also play a role. Several *C. albicans* HDACs participate in decrotonylation of H3K9cr. H3K9cr was co-regulated with H3K9ac in HAT and HDAC mutants, when pan-HDAC inhibitors were used and in response to metabolic and cell wall stress. Previous results in *S. cerevisiae* and mammals are consistent with our data in *C. albicans*, showing that histone crotonylation and acetylation are co-regulated and performed by a similar set of enzymes (Andrews et al., 2016a; Sabari et al., 2015).

Our study further establishes a prominent role for the YEATS crotonylation readers Taf14 and Yaf9 in pathogen fitness *in vitro* and *in vivo* to control virulence of *C. albicans*. Detailed analyses showed that Taf14 plays a role in two pathways critical for host interactions and pathogenicity: cell wall integrity and invasive hyphal growth. Our conclusion is supported by a *C. albicans* mutant library screen showing defective adherence of *taf14Δ/Δ* to silicone (Finkel et al., 2012). Our transcriptional data provide a possible mechanism behind these cell wall-related phenotypes. A number of key cell wall genes are differentially expressed in *taf14Δ/Δ* cells and the cell wall stress-responsive transcriptional program is constitutively "on" without exogenous stress. Also, the mutant displays enhanced activation of cell wall integrity pathways. These transcriptional and signaling changes could "prime" the mutant for facing exogenous cell wall stress, resulting in the observed resistance. Additional mechanisms likely contribute, as the W80A mutant is cell wall stress resistant (although less than *taf14Δ/Δ*), but did not show activation of the stress-responsive cell wall genes that we tested (*PHR1*, *KRE1*, and *EXG2*).

Phenotypes of the W80A mutant show that the chromatin reader function of *C. albicans* Taf14 mediates cell wall gene expression, stress responses, and invasive filamentation. *C. albicans* Taf14 interacts robustly with H3K9cr, whereas its binding to H3K9ac is much less pronounced. Consistent with our data, *S. cerevisiae* Taf14 can interact with acetyl-lysine, but its strongest interaction partner is crotonyl-lysine (Klein et al., 2018). The H3K9cr mark is present at promoter regions of Taf14-dependent cell wall genes *ALS1* and *HWP1*, both of which are induced by

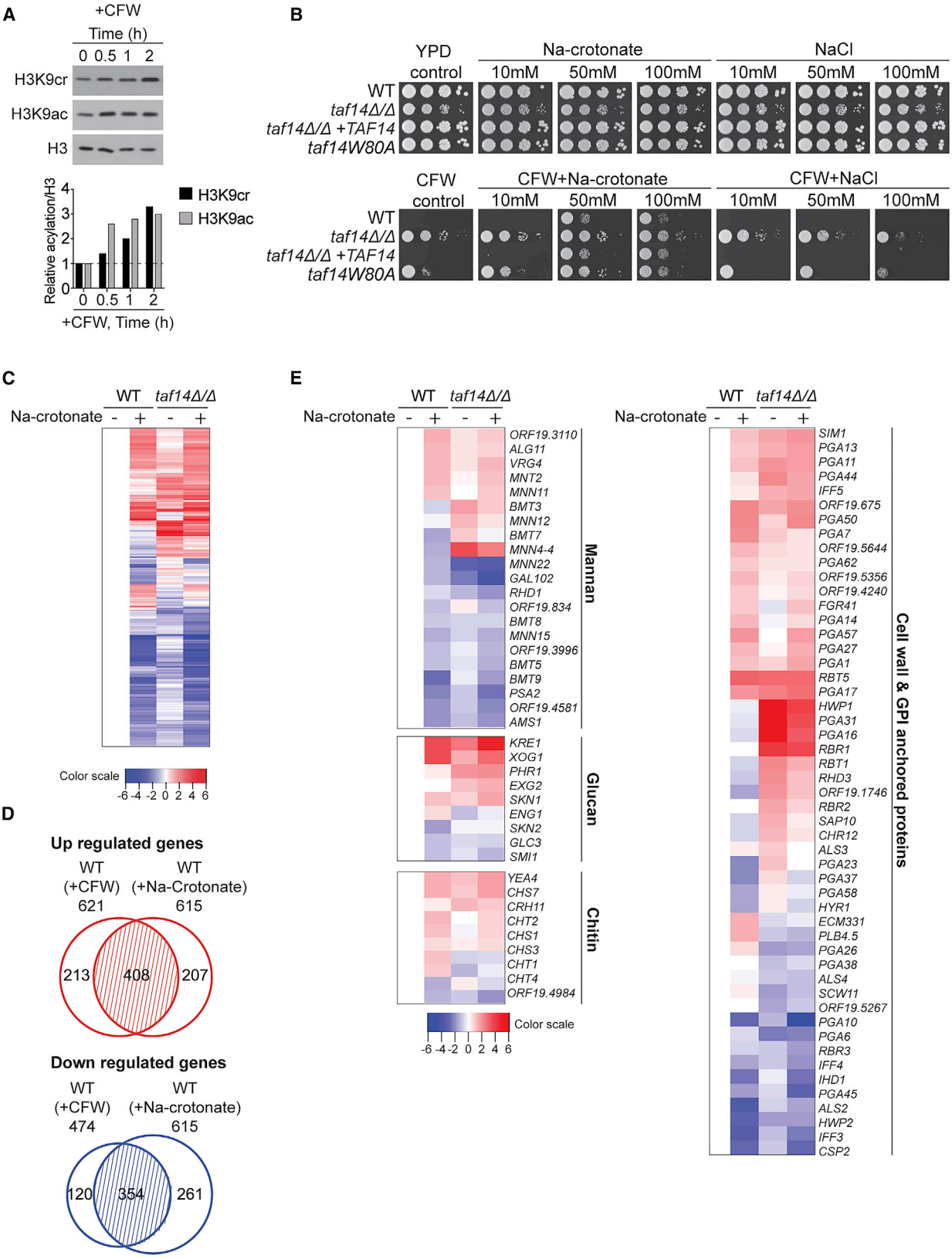

(legend on next page)

the filamentous program. Although CFW treatment elevates the levels of H3K9cr in chromatin, this is not the case in *ALS1* and *HWP1* promoter regions, arguing for distinct stress-regulated dynamics of histone crotonylation at specific genes. Blocking the C-terminal domain of Taf14, which is needed for interactions with chromatin and transcriptional complexes, also results in cell wall and filamentation phenotypes. Blocking the C-terminal domain further leads to fitness defects and reduced virulence, phenocopying the deletion of the *TAF14* gene, although the W80A mutant shows normal fitness *in vitro* and *in vivo*. We conclude that the C-terminal domain is especially important for virulence of *C. albicans* in the disseminated infection model.

In summary, our findings expand the roles and metabolic signals for histone crotonylation and the YEATS readers in eukaryotes and suggest that diverse histone acylations could control metabolic adaptation and stress susceptibility of eukaryotic commensal/pathogens such as *C. albicans*. Bacteria-derived butyrate regulates histone crotonylation of mammalian gut cells (Fellows et al., 2018). We now show that butyrate and crotonate regulate the levels of histone crotonylation in *C. albicans*. Thus, these short-chain fatty acids may have broad effects on the interactions of the bacterial microbiome with both eukaryotic mycobiomes and host cells. By showing that the *C. albicans* YEATS mutants *taf14Δ/Δ* and *yaf9Δ/Δ* are hypovirulent in the mouse systemic infection model, our study has implications for combatting fungal diseases, a global health issue with limited treatment options (Brown et al., 2012; Pappas et al., 2018). Although YEATS inhibitors are emerging for possible future applications in cancer biology (Christott et al., 2018; Li et al., 2018b; Moustakim et al., 2018), our work suggests that the situation with fungal YEATS proteins is distinct to their mammalian counterparts. Instead of targeting the YEATS domain, any attempt to target Taf14 for antifungal therapy should focus on blocking the C-terminal domain, which mediates interactions with transcriptional and chromatin complexes and drives pathogenicity. Our bioinformatics data demonstrate that the YEATS proteins are conserved in human fungal pathogens, suggesting that their inhibition could be broadly promising.

STAR★METHODS

Detailed methods are provided in the online version of this paper and include the following:

- KEY RESOURCES TABLE
- LEAD CONTACT AND MATERIALS AVAILABILITY
- EXPERIMENTAL MODEL AND SUBJECT DETAILS
  - *Candida* strains and growth conditions
  - Mice
- METHOD DETAILS
  - Strain construction
  - Zymolyase Treatment
  - Microscopy
  - RNA-seq analysis of gene expression
  - qPCR analysis of gene expression
  - Chromatin immunoprecipitation (ChIP)
  - Murine infection model
  - Western blot analysis
  - Dot blot analysis
  - Binding assays of Taf14 with H3K9cr and H3K9ac peptides
  - Bioinformatic analysis
- QUANTIFICATION AND STATISTICAL ANALYSIS
- DATA AND CODE AVAILABILITY

SUPPLEMENTAL INFORMATION

Supplemental Information can be found online at https://doi.org/10.1016/j.celrep.2020.107528.

ACKNOWLEDGMENTS

This work was supported by project grants from the Australian National Health and Medical Research Council (APP1138812 and APP1158687 to A.T. and J.V.) and the Croatian Unity Through Knowledge Fund (to A.T. and M. Sopta). A.T. and T.H.B. are supported by Australian Research Council Future Fellowships (FT190100733 and FT180100049). K.K. was supported in part by projects from the Austrian Science Fund (FWF-SFB70-08-B30 and FWF-P-32582-B22). M.T. was supported in part by an FWF Erwin Schrödinger Fellowship (FWF-J-03835). We acknowledge the support of the Monash Bioinformatics Platform and the Monash Animal Research Platform, and we thank Samantha O'Dea for assistance with animal experiments.

AUTHOR CONTRIBUTIONS

J.V., Q.W., N.V., and A.T. designed research. J.V., Q.W., T.M.T., T.L.L., and A.S. performed research. N.V. contributed to strain construction, experimental characterization of the mutant strains, and general direction of the project. Y.W., P.F.H., M. See, J.S., and D.R.P. performed or supervised the bioinformatics analyses of the RNA-seq data or YEATS protein distribution in fungi and provided advice on statistical analyses. M.T. and K.K. provided tools (a library of chromatin modification mutants). K.K. redacted the manuscript. M. Sopta and T.H.B. advised on experiments and provided intellectual input into the project. J.V., Q.W., T.H.B., and A.T. analyzed the data. A.T., J.V., and M. Sopta obtained funding. A.T. wrote the paper with assistance from J.V. and Q.W. and input from the other authors.

Figure 7. The SCFA Crotonate Has Broad-Ranging Effects on *C. albicans* Gene Expression and Cell Wall Stress Responses

(A) Western blot analysis of histone acylations were performed as in Figure 1A. Log phase grown cultures were treated with 20 μg/mL calcofluor white (CFW) for the indicated time points. Bar graph shows quantification of the levels of H3K9cr or H3K9ac normalized to the H3 control. The 0 h sample was set to 1, and all other values were calculated relative to that. Ponceau-stained membranes are shown in Figure S1H, and uncropped western blots are shown in Figure S6H.

(B) Ten-fold serial dilutions of cultures of the indicated *C. albicans* strains were grown on YPD plates in the presence or absence of 30 μg/mL CFW, with or without Na-crotonate or NaCl at the indicated doses. Images were taken after 2 days of growth at 30°C.

(C) Heatmap showing changes in expression of differentially regulated genes in crotonate-treated WT, as well as untreated and crotonate-treated *taf14Δ/Δ*, all relative to untreated WT (FDR $\leq$ 0.01, $\log_2 = 2$). The entire gene list is in Data S2 and can be interactively viewed at http://rnasystems.erc.monash.edu/2019/verma_et-al/.

(D) Venn diagram showing the overlap of genes differentially expressed in CFW-treated WT versus crotonate-treated WT (FDR < 0.01 and $\log_2 = 1$ were used as cutoffs). The gene list used to construct the Venn diagram is in Data S2.

(E) Heatmaps showing changes in gene expression of cell wall-related genes relative to untreated WT (FDR $\leq$ 0.01, $\log_2 = 1$).

DECLARATION OF INTERESTS

The authors declare no competing interests.

Received: July 31, 2019
Revised: January 31, 2020
Accepted: March 27, 2020
Published: April 21, 2020

REFERENCES

Andrews, F.H., Shinsky, S.A., Shanle, E.K., Bridgers, J.B., Gest, A., Tsun, I.K., Krajewski, K., Shi, X., Strahl, B.D., and Kutateladze, T.G. (2016a). The Taf14 YEATS domain is a reader of histone crotonylation. Nat. Chem. Biol. *12*, 396–398.

Andrews, F.H., Strahl, B.D., and Kutateladze, T.G. (2016b). Insights into newly discovered marks and readers of epigenetic information. Nat. Chem. Biol. *12*, 662–668.

Ballou, E.R., Avelar, G.M., Childers, D.S., Mackie, J., Bain, J.M., Wagener, J., Kastora, S.L., Panea, M.D., Hardison, S.E., Walker, L.A., et al. (2016). Lactate signalling regulates fungal β-glucan masking and immune evasion. Nat. Microbiol. *2*, 16238.

Brown, G.D., Denning, D.W., Gow, N.A., Levitz, S.M., Netea, M.G., and White, T.C. (2012). Hidden killers: human fungal infections. Sci. Transl. Med. *4*, 165rv13.

Brown, A.J., Brown, G.D., Netea, M.G., and Gow, N.A. (2014). Metabolism impacts upon Candida immunogenicity and pathogenicity at multiple levels. Trends Microbiol. *22*, 614–622.

Chen, Y., Sprung, R., Tang, Y., Ball, H., Sangras, B., Kim, S.C., Falck, J.R., Peng, J., Gu, W., and Zhao, Y. (2007). Lysine propionylation and butyrylation are novel post-translational modifications in histones. Mol. Cell. Proteomics *6*, 812–819.

Christott, T., Bennett, J., Coxon, C., Monteiro, O., Giroud, C., Beke, V., Felce, S.L., Gamble, V., Gileadi, C., Poda, G., et al. (2018). Discovery of a selective inhibitor for the YEATS domains of ENL/AF9. SLAS Discov. *24*, 133–141.

Côte, P., Hogues, H., and Whiteway, M. (2009). Transcriptional analysis of the Candida albicans cell cycle. Mol. Biol. Cell *20*, 3363–3373.

Dahan, O., and Kupiec, M. (2004). The Saccharomyces cerevisiae gene CDC40/PRP17 controls cell cycle progression through splicing of the ANC1 gene. Nucleic Acids Res. *32*, 2529–2540.

Dai, L., Peng, C., Montellier, E., Lu, Z., Chen, Y., Ishii, H., Debernardi, A., Buchou, T., Rousseaux, S., Jin, F., et al. (2014). Lysine 2-hydroxyisobutyrylation is a widely distributed active histone mark. Nat. Chem. Biol. *10*, 365–370.

Dutta, A., Abmayr, S.M., and Workman, J.L. (2016). Diverse activities of histone acylations connect metabolism to chromatin function. Mol. Cell *63*, 547–552.

Ene, I.V., Adya, A.K., Wehmeier, S., Brand, A.C., MacCallum, D.M., Gow, N.A., and Brown, A.J. (2012). Host carbon sources modulate cell wall architecture, drug resistance and virulence in a fungal pathogen. Cell. Microbiol. *14*, 1319–1335.

Feigerle, J.T., and Weil, P.A. (2016). The C terminus of the RNA polymerase II transcription factor IID (TFIID) subunit Taf2 mediates stable association of subunit Taf14 into the yeast TFIID complex. J. Biol. Chem. *291*, 22721–22740.

Fellows, R., Denizot, J., Stellato, C., Cuomo, A., Jain, P., Stoyanova, E., Balázsi, S., Hajnády, Z., Liebert, A., Kazakevych, J., et al. (2018). Microbiota derived short chain fatty acids promote histone crotonylation in the colon through histone deacetylases. Nat. Commun. *9*, 105.

Finkel, J.S., Xu, W., Huang, D., Hill, E.M., Desai, J.V., Woolford, C.A., Nett, J.E., Taff, H., Norice, C.T., Andes, D.R., et al. (2012). Portrait of Candida albicans adherence regulators. PLoS Pathog. *8*, e1002525.

Flynn, E.M., Huang, O.W., Poy, F., Oppikofer, M., Bellon, S.F., Tang, Y., and Cochran, A.G. (2015). A subset of human bromodomains recognizes butyryllysine and crotonyllysine histone peptide modifications. Structure *23*, 1801–1814.

Gowans, G.J., Bridgers, J.B., Zhang, J., Dronamraju, R., Burnetti, A., King, D.A., Thiengmany, A.V., Shinsky, S.A., Bhanu, N.V., Garcia, B.A., et al. (2019). Recognition of histone crotonylation by Taf14 links metabolic state to gene expression. Mol. Cell *76*, 909–921.e3.

Grahl, N., Demers, E.G., Lindsay, A.K., Harty, C.E., Willger, S.D., Piispanen, A.E., and Hogan, D.A. (2015). Mitochondrial activity and Cyr1 are key regulators of Ras1 activation of C. albicans virulence pathways. PLoS Pathog. *11*, e1005133.

Harrison, P.F., Powell, D.R., Clancy, J.L., Preiss, T., Boag, P.R., Traven, A., Seemann, T., and Beilharz, T.H. (2015). PAT-seq: a method to study the integration of 3′-UTR dynamics with gene expression in the eukaryotic transcriptome. RNA *21*, 1502–1510.

Hernday, A.D., Noble, S.M., Mitrovich, Q.M., and Johnson, A.D. (2010). Genetics and molecular biology in Candida albicans. Methods Enzymol. *470*, 737–758.

Huang, H., Wang, D.L., and Zhao, Y. (2018). Quantitative crotonylome analysis expands the roles of p300 in the regulation of lysine crotonylation pathway. Proteomics *18*, e1700230.

Klein, B.J., Vann, K.R., Andrews, F.H., Wang, W.W., Zhang, J., Zhang, Y., Beloglazkina, A.A., Mi, W., Li, Y., Li, H., et al. (2018). Structural insights into the π-π-π stacking mechanism and DNA-binding activity of the YEATS domain. Nat. Commun. *9*, 4574.

Koch, B., Barugahare, A.A., Lo, T.L., Huang, C., Schittenhelm, R.B., Powell, D.R., Beilharz, T.H., and Traven, A. (2018). A metabolic checkpoint for the yeast-to-hyphae developmental switch regulated by endogenous nitric oxide signaling. Cell Rep. *25*, 2244–2258.e7.

Lavoie, H., Sellam, A., Askew, C., Nantel, A., and Whiteway, M. (2008). A toolbox for epitope-tagging and genome-wide location analysis in Candida albicans. BMC Genomics *9*, 578.

Li, Y., Sabari, B.R., Panchenko, T., Wen, H., Zhao, D., Guan, H., Wan, L., Huang, H., Tang, Z., Zhao, Y., et al. (2016). Molecular coupling of histone crotonylation and active transcription by AF9 YEATS domain. Mol. Cell *62*, 181–193.

Li, X., Egervari, G., Wang, Y., Berger, S.L., and Lu, Z. (2018a). Regulation of chromatin and gene expression by metabolic enzymes and metabolites. Nat. Rev. Mol. Cell Biol. *19*, 563–578.

Li, X., Li, X.M., Jiang, Y., Liu, Z., Cui, Y., Fung, K.Y., van der Beelen, S.H.E., Tian, G., Wan, L., Shi, X., et al. (2018b). Structure-guided development of YEATS domain inhibitors by targeting π-π-π stacking. Nat. Chem. Biol. *14*, 1140–1149.

Lindsay, A.K., Morales, D.K., Liu, Z., Grahl, N., Zhang, A., Willger, S.D., Myers, L.C., and Hogan, D.A. (2014). Analysis of Candida albicans mutants defective in the Cdk8 module of mediator reveal links between metabolism and biofilm formation. PLoS Genet. *10*, e1004567.

Lorenz, M.C., Bender, J.A., and Fink, G.R. (2004). Transcriptional response of Candida albicans upon internalization by macrophages. Eukaryot. Cell *3*, 1076–1087.

Morales, D.K., Grahl, N., Okegbe, C., Dietrich, L.E., Jacobs, N.J., and Hogan, D.A. (2013). Control of Candida albicans metabolism and biofilm formation by Pseudomonas aeruginosa phenazines. MBio *4*, e00526–e12.

Moustakim, M., Christott, T., Monteiro, O.P., Bennett, J., Giroud, C., Ward, J., Rogers, C.M., Smith, P., Panagakou, I., Díaz-Sáez, L., et al. (2018). Discovery of an MLLT1/3 YEATS domain chemical probe. Angew. Chem. Int. Engl. *57*, 16302–16307.

Noble, S.M., and Johnson, A.D. (2005). Strains and strategies for large-scale gene deletion studies of the diploid human fungal pathogen Candida albicans. Eukaryot. Cell *4*, 298–309.

Noble, S.M., French, S., Kohn, L.A., Chen, V., and Johnson, A.D. (2010). Systematic screens of a Candida albicans homozygous deletion library decouple morphogenetic switching and pathogenicity. Nat. Genet. *42*, 590–598.

Pappas, P.G., Lionakis, M.S., Arendrup, M.C., Ostrosky-Zeichner, L., and Kullberg, B.J. (2018). Invasive candidiasis. Nat. Rev. Dis. Primers *4*, 18026.

Pérez, J.C., Kumamoto, C.A., and Johnson, A.D. (2013). Candida albicans commensalism and pathogenicity are intertwined traits directed by a tightly knit transcriptional regulatory circuit. PLoS Biol. *11*, e1001510.

Pradhan, A., Avelar, G.M., Bain, J.M., Childers, D.S., Larcombe, D.E., Netea, M.G., Shekhova, E., Munro, C.A., Brown, G.D., Erwig, L.P., et al. (2018). Hypoxia promotes immune evasion by triggering β-glucan masking on the Candida albicans cell surface via mitochondrial and cAMP-protein kinase A signaling. mBio *9*, e01318-18.

Ritchie, M.E., Phipson, B., Wu, D., Hu, Y., Law, C.W., Shi, W., and Smyth, G.K. (2015). limma powers differential expression analyses for RNA-sequencing and microarray studies. Nucleic Acids Res. *43*, e47.

Robinson, M.D., and Oshlack, A. (2010). A scaling normalization method for differential expression analysis of RNA-seq data. Genome Biol. *11*, R25.

Ruijter, J.M., Ramakers, C., Hoogaars, W.M., Karlen, Y., Bakker, O., van den Hoff, M.J., and Moorman, A.F. (2009). Amplification efficiency: linking baseline and bias in the analysis of quantitative PCR data. Nucleic Acids Res. *37*, e45.

Sabari, B.R., Tang, Z., Huang, H., Yong-Gonzalez, V., Molina, H., Kong, H.E., Dai, L., Shimada, M., Cross, J.R., Zhao, Y., et al. (2015). Intracellular crotonyl-CoA stimulates transcription through p300-catalyzed histone crotonylation. Mol. Cell *58*, 203–215.

Schulze, J.M., Wang, A.Y., and Kobor, M.S. (2009). YEATS domain proteins: a diverse family with many links to chromatin modification and transcription. Biochem. Cell Biol. *87*, 65–75.

Schulze, J.M., Kane, C.M., and Ruiz-Manzano, A. (2010). The YEATS domain of Taf14 in Saccharomyces cerevisiae has a negative impact on cell growth. Mol. Genet. Genomics *283*, 365–380.

Shanle, E.K., Andrews, F.H., Meriesh, H., McDaniel, S.L., Dronamraju, R., DiFiore, J.V., Jha, D., Wozniak, G.G., Bridgers, J.B., Kerschner, J.L., et al. (2015). Association of Taf14 with acetylated histone H3 directs gene transcription and the DNA damage response. Genes Dev. *29*, 1795–1800.

Shen, J., Guo, W., and Köhler, J.R. (2005). CaNAT1, a heterologous dominant selectable marker for transformation of Candida albicans and other pathogenic Candida species. Infect. Immun. *73*, 1239–1242.

Shivarathri, R., Tscherner, M., Zwolanek, F., Singh, N.K., Chauhan, N., and Kuchler, K. (2019). The Fungal Histone Acetyl Transferase Gcn5 Controls Virulence of the Human Pathogen *Candida albicans* through Multiple Pathways. Sci. Rep. *9*, 9445.

Silao, F.G.S., Ward, M., Ryman, K., Wallström, A., Brindefalk, B., Udekwu, K., and Ljungdahl, P.O. (2019). Mitochondrial proline catabolism activates Ras1/cAMP/PKA-induced filamentation in Candida albicans. PLoS Genet. *15*, e1007976.

Simithy, J., Sidoli, S., Yuan, Z.F., Coradin, M., Bhanu, N.V., Marchione, D.M., Klein, B.J., Bazilevsky, G.A., McCullough, C.E., Magin, R.S., et al. (2017). Characterization of histone acylations links chromatin modifications with metabolism. Nat. Commun. *8*, 1141.

Tan, M., Luo, H., Lee, S., Jin, F., Yang, J.S., Montellier, E., Buchou, T., Cheng, Z., Rousseaux, S., Rajagopal, N., et al. (2011). Identification of 67 histone marks and histone lysine crotonylation as a new type of histone modification. Cell *146*, 1016–1028.

Tucey, T.M., Verma-Gaur, J., Nguyen, J., Hewitt, V.L., Lo, T.L., Shingu-Vazquez, M., Robertson, A.A., Hill, J.R., Pettolino, F.A., Beddoe, T., et al. (2016). The endoplasmic reticulum-mitochondrion tether ERMES orchestrates fungal immune evasion, illuminating inflammasome responses to hyphal signals. mSphere *1*, e00074-16.

Tscherner, M., Stappler, E., Hnisz, D., and Kuchler, K. (2012). The histone acetyltransferase Hat1 facilitates DNA damage repair and morphogenesis in *Candida albicans*. Mol. Microbiol. *86*, 1197–1214.

Tucey, T.M., Verma, J., Harrison, P.F., Snelgrove, S.L., Lo, T.L., Scherer, A.K., Barugahare, A.A., Powell, D.R., Wheeler, R.T., Hickey, M.J., et al. (2018). Glucose homeostasis is important for immune cell viability during Candida challenge and host survival of systemic fungal infection. Cell Metab. *27*, 988–1006.e7.

Uwamahoro, N., Verma-Gaur, J., Shen, H.H., Qu, Y., Lewis, R., Lu, J., Bambery, K., Masters, S.L., Vince, J.E., Naderer, T., and Traven, A. (2014). The pathogen Candida albicans hijacks pyroptosis for escape from macrophages. mBio *5*, e00003-14.

Verma-Gaur, J., Qu, Y., Harrison, P.F., Lo, T.L., Quenault, T., Dagley, M.J., Bellousoff, M., Powell, D.R., Beilharz, T.H., and Traven, A. (2015). Integration of posttranscriptional gene networks into metabolic adaptation and biofilm maturation in Candida albicans. PLoS Genet. *11*, e1005590.

Wang, X., Zhu, W., Chang, P., Wu, H., Liu, H., and Chen, J. (2018). Merge and separation of NuA4 and SWR1 complexes control cell fate plasticity in *Candida albicans*. Cell Discov. *4*, 45.

Warnes, G.R., Bolker, B., Bonebakker, L., Gentleman, R., Huber, W., Liaw, A., Lumley, T., Maechler, M., Magnusson, A., Moeller, S., et al. (2019). gplots: various R programming tools for plotting data, version 3.0.1.1.https://cran.r-project.org/web/packages/gplots/index.html.

Xie, Z., Dai, J., Dai, L., Tan, M., Cheng, Z., Wu, Y., Boeke, J.D., and Zhao, Y. (2012). Lysine succinylation and lysine malonylation in histones. Mol. Cell. Proteomics *11*, 100–107.

Xie, J., Jenull, S., Tscherner, M., and Kuchler, K. (2016). The Paralogous Histone Deacetylases Rpd3 and Rpd31 Play Opposing Roles in Regulating the White-Opaque Switch in the Fungal Pathogen *Candida albicans*. mBio *7*, e01807.

Xie, Z., Zhang, D., Chung, D., Tang, Z., Huang, H., Dai, L., Qi, S., Li, J., Colak, G., Chen, Y., et al. (2016). Metabolic regulation of gene expression by histone lysine β-hydroxybutyrylation. Mol. Cell *62*, 194–206.

Xiong, X., Panchenko, T., Yang, S., Zhao, S., Yan, P., Zhang, W., Xie, W., Li, Y., Zhao, Y., Allis, C.D., and Li, H. (2016). Selective recognition of histone crotonylation by double PHD fingers of MOZ and DPF2. Nat. Chem. Biol. *12*, 1111–1118.

Zavrel, M., Majer, O., Kuchler, K., and Rupp, S. (2012). Transcription factor Efg1 shows a haploinsufficiency phenotype in modulating the cell wall architecture and immunogenicity of Candida albicans. Eukaryot. Cell *11*, 129–140.

Zhao, D., Guan, H., Zhao, S., Mi, W., Wen, H., Li, Y., Zhao, Y., Allis, C.D., Shi, X., and Li, H. (2016). YEATS2 is a selective histone crotonylation reader. Cell Res. *26*, 629–632.

Zhao, D., Li, Y., Xiong, X., Chen, Z., and Li, H. (2017). YEATS domain-A histone acylation reader in health and disease. J. Mol. Biol. *429*, 1994–2002.

STAR★METHODS

KEY RESOURCES TABLE

REAGENT or RESOURCE	SOURCE	IDENTIFIER
Antibodies		
Pan anti-crotonyllysine antibody	PTM Biolabs	Cat# PTM501
Anti-crotonyl-Histone H3 (Lys9) antibody	PTM Biolabs	Cat# PTM516
Anti-acetyl-Histone H3 (Lys9) antibody	EMD Millipore	Cat# 07-352; RRID:AB_310544
Anti-histone H3 antibody	Abcam	Cat# ab1791; RRID:AB_302613
Anti-Taf14 antibody	GeneTex	Cat# GTX64177
Phospho-p44/42 MAPK (Erk1/2) (Thr202/Tyr204)	Cell Signaling	Cat# 9101S
Anti-Actin Antibody, clone C4	Millipore	Cat # MAB1501; RRID:AB_2223041
Anti-Rabbit IgG	Sigma	Cat # A0504
Anti-Mouse IgG	Sigma	Cat # A4416; RRID:AB_258167
Chemicals, Peptides, and Recombinant Proteins		
Crotonic acid	Sigma	Cat# 113018
Sodium butyrate	Sigma	Cat# 303410
Trichostatin A (TSA)	Sigma	Cat# T8552
Calcofluor white (CFW)	Sigma	Cat# F3543
Trichloroacetic acid (TCA)	Sigma	Cat# T6399
SuperBlock	Thermo Scientific	Cat# 37537
H3 (1-19): BiotinAhx-ARTKQTARKSTGGKAPRKQ	Mimotopes	N/A
H3K9ac: BiotinAhx-ARTKQTARKacSTGGKAPRKQ	Mimotopes	N/A
H3K9cr: BiotinAhx-ARTKQTARKcrSTGGKAPRKQ	Mimotopes	N/A
H3K9bu: BiotinAhx-ARTKQTARKbuSTGGKAPRKQ	Mimotopes	N/A
Critical Commercial Assays		
Amersham ECL western blotting detection reagent	Sigma	Cat# RPN2209
Clarity Western ECL substrate	Biorad	Cat# 1705060
Deposited Data		
RNA-seq data (CFW experiment in Figure 4)	This paper	GSE128279
RNA-seq data (Crotonate experiment in Figure 7)	This paper	GSE141229
Experimental Models: Organisms/Strains		
Mouse: BALB/c	Monash Animal Services (Melbourne, Australia)	N/A
C. albicans: SN152, *leu2Δ/leu2Δ, arg4Δ/arg4Δ, his1Δ/his1Δ, ura3Δ/URA3, iro1Δ/IRO1*	Noble et al., 2010	YCAT638
C. albicans: SN425. *leu2Δ::C.d.HIS1/leu2Δ::C.m.LEU2, arg4Δ/arg4Δ::C.d.ARG4, his1Δ/his1Δ, ura3Δ/URA3, iro1Δ/IRO1*	Noble et al., 2010	YCAT641

(*Continued on next page*)

Continued

REAGENT or RESOURCE	SOURCE	IDENTIFIER
C. albicans: *TAF14/taf14Δ. TAF14/taf14Δ::C.m.LEU2, arg4Δ/arg4Δ, leu2Δ/leu2Δ, his1Δ/his1Δ, ura3Δ/URA3, iro1Δ/IRO1*	This study	YCAT856
C. albicans: *taf14Δ/Δ+ TAF14* (1X). *leu2Δ/leu2Δ::TAF14::C.d.ARG4, taf14Δ::C.d.HIS1/ taf14Δ::C.m.LEU2, his1Δ/his1Δ, arg4Δ/arg4Δ, ura3Δ/URA3, iro1Δ/IRO1*	This study	YCAT871
C. albicans: *taf14Δ/Δ. taf14Δ::C.d.HIS1/taf14Δ::C.m.LEU2, arg4Δ/arg4Δ, leu2Δ/leu2Δ::C.d.ARG4, his1Δ/his1Δ, ura3Δ/URA3, iro1Δ/IRO1*	This study	YCAT877 YCAT878 YCAT879
C. albicans: Taf14-TAP. *TAF14::TAP::ARG4/TAF14::TAP::HIS1, leu2Δ/leu2Δ, arg4Δ/arg4Δ, his1Δ/his1Δ, ura3Δ/URA3, iro1Δ/IRO1*	This study	YCAT882, YCAT883
C. albicans: *taf14Δ/Δ+ TAF14* (2X). *leu2Δ/leu2Δ::TAF14::C.d.ARG4, taf14Δ::TAF14::p-A.g.TEF1- C.a.NAT1-t-A.g.TEF1::C.d.HIS1/ taf14Δ::C.m.LEU2, his1Δ/his1Δ, arg4Δ/arg4Δ, ura3Δ/URA3, iro1Δ/IRO1*	This study	YCAT950
C. albicans: *taf14Δ/Δ+ TAF14. leu2Δ/leu2Δ::TAF14* without intron*::C.d.ARG4, taf14Δ::TAF14* without intron*:: p-A.g.TEF1-C.a.NAT1-t A.g.TEF1::C.d.HIS1/ taf14Δ::C.m.LEU2, his1Δ/his1Δ, arg4Δ/arg4Δ, ura3Δ/URA3, iro1Δ/IRO1*	This study	YCAT964
C. albicans: *taf14W80A. leu2Δ/leu2Δ::taf14W80A* without intron*::C.d.ARG4, taf14Δ::Taf14W80A* without intron*:: p-A.g.TEF1-C.a.NAT1-t A.g.TEF1::C.d.HIS1/ taf14Δ::C.m.LEU2, his1Δ/his1Δ, arg4Δ/arg4Δ, ura3Δ/URA3, iro1Δ/IRO1*	This study	YCAT969
C. albicans: *yaf9Δ/Δ. yaf9Δ::C.d.HIS1/ yaf9Δ::C.m.LEU2, arg4Δ/arg4Δ, leu2Δ/leu2Δ::C.d.ARG4, his1Δ/his1Δ, ura3Δ/URA3, iro1Δ/IRO1*	This study	YCAT972, YCAT973
C. albicans: *yaf9Δ/Δ + YAF9. leu2Δ/leu2Δ::YAF9::C.d.ARG4, yaf9Δ::C.d.HIS1/ yaf9Δ::C.m.LEU2, his1Δ/his1Δ, arg4Δ/arg4Δ, ura3Δ/URA3, iro1Δ/IRO1*	This study	YCAT975
C. albicans: SC5314	From K. Kuchler's lab	YCAT1019
C. albicans: *rtt109Δ/Δ. rtt109Δ::FRT/rtt109Δ::FRT*	Tscherner et al., 2012	YCAT1022
C. albicans: *rtt109Δ/Δ hat1Δ/Δ. hat1Δ::FRT/hat1Δ::FRT, rtt109Δ::FRT/rtt109Δ::FRT*	Tscherner et al., 2012	YCAT1023
C. albicans: *hat1Δ/Δ. hat1Δ::FRT/hat1Δ::FRT*	Tscherner et al., 2012	YCAT1024
C. albicans: *hat2Δ/Δ. hat2Δ::FRT/hat2Δ::SAT1*	Tscherner et al., 2012	YCAT1025

(*Continued on next page*)

Continued

REAGENT or RESOURCE	SOURCE	IDENTIFIER
C. albicans: *hat1Δ/Δ hat2Δ/Δ. hat1Δ::FRT/hat1Δ::FRT, hat2Δ::FRT/hat2Δ::SAT1*	Tscherner et al., 2012	YCAT1026
C. albicans: *gcn5Δ/Δ. gcn5Δ/gcn5Δ::NAT1*	Shivarathri et al., 2019	YCAT1027
C. albicans: *gcn5Δ/Δ hat1Δ/Δ. hat1Δ/hat1Δ, gcn5Δ/gcn5Δ::NAT1*	From K. Kuchler's lab, unpublished	YCAT1028
C. albicans: *gcn5Δ/Δ rtt109Δ/Δ. rtt109Δ/ rtt109Δ, gcn5Δ::FRT/gcn5Δ::FRT*	From K. Kuchler's lab, unpublished	YCAT1030
C. albicans: *gcn5Δ/Δ rtt109Δ/Δ hat1Δ/Δ. hat1Δ/hat1Δ, rtt109Δ/rtt109Δ, gcn5Δ::FRT/gcn5Δ::FRT*	From K. Kuchler's lab, unpublished	YCAT1031
C. albicans: *J4-2.1. leu2Δ::FRT/leu2Δ::FRT, his1Δ::FRT/his1Δ::FRT*	Xie et al., 2016	YCAT1032
C. albicans: *hda1Δ/Δ. hda1Δ::C.m.LEU2/hda1Δ::C.d.HIS1*	Xie et al., 2016	YCAT1033
C. albicans: *hst2Δ/Δ. hst2Δ::C.m.LEU2/hst2Δ::C.d.HIS1*	Xie et al., 2016	YCAT1034
C. albicans: *hos1Δ/Δ. hos1Δ::C.m.LEU2/hos1Δ::C.d.HIS1*	Xie et al., 2016	YCAT1035
C. albicans: *hos3Δ/Δ. hos3Δ::C.m.LEU2/hos3Δ::C.d.HIS1*	Xie et al., 2016	YCAT1036
C. albicans: *hos2Δ/Δ. hos2Δ::C.m.LEU2/hos2Δ::C.d.HIS1*	Xie et al., 2016	YCAT1037
C. albicans: *hpa2Δ/Δ. hpa2Δ::C.m.LEU2/hpa2Δ::C.d.HIS1*	Xie et al., 2016	YCAT1038
C. albicans: *nat4Δ/Δ. nat4Δ::C.m.LEU2/nat4Δ::C.d.HIS1*	Xie et al., 2016	YCAT1039
C. albicans: *hst1Δ/Δ. hst1Δ::C.m.LEU2/hst1Δ::C.d.HIS1*	Xie et al., 2016	YCAT1040
C. albicans: *rpd3Δ/Δ. rpd3Δ::C.m.LEU2/rpd3Δ::C.d.HIS1*	Xie et al., 2016	YCAT1041
C. albicans: *sas2Δ/Δ. sas2Δ::C.m.LEU2/sas2Δ::C.d.HIS1*	Xie et al., 2016	YCAT1042
C. albicans: *elp3Δ/Δ. elp3Δ::C.m.LEU2/elp3Δ::C.d.HIS1*	Xie et al., 2016	YCAT1043
C. albicans: *sir2Δ/Δ. sir2Δ::C.m.LEU2/sir2Δ::C.d.HIS1*	Xie et al., 2016	YCAT1044
C. albicans: *spt10Δ/Δ. spt10Δ::C.m.LEU2/spt10Δ::C.d.HIS1*	Xie et al., 2016	YCAT1045
C. albicans: *set3Δ/Δ. set3Δ::C.m.LEU2/set3Δ::C.d.HIS1*	Xie et al., 2016	YCAT1046
C. albicans: *rpd3Δ/Δrpd31Δ/Δ. rpd3Δ::C.d.HIS1/rpd3Δ::C.m.LEU2, rpd31Δ::FRT/rpd31Δ::SAT1*	Xie et al., 2016	YCAT1047
Oligonucleotides		
See Table S1	IDT	N/A
Software and Algorithms		
ImageQuant v7.0	GE Healthcare	http://www.gelifesciences.com/en/us/
HMMER (software version of 3.1)	N/A	http://hmmer.org/download.html
ImageJ 1.52a	NIH	https://imagej.nih.gov/ij/download.html

(*Continued on next page*)

Continued

REAGENT or RESOURCE	SOURCE	IDENTIFIER
Tail Tools	Harrison et al., 2015	https://github.com/Monash-RNA-Systems-Biology-Laboratory/tail-tools
R package edgeR	Robinson and Oshlack, 2010	https://bioconductor.org/packages/release/bioc/html/edgeR.html
R package limma	N/A	http://bioinf.wehi.edu.au/limma/
R package fitnoise	N/A	https://github.com/pfh/fitnoise
R package gplots	N/A	https://cran.r-project.org/web/packages/gplots/index.html
LinReg PCR software	Ruijter et al., 2009	N/A
GraphPad Prism v 8	GraphPad software	https://www.graphpad.com/scientific-software/prism/

LEAD CONTACT AND MATERIALS AVAILABILITY

Further information and requests for resources and reagents should be directed to and will be fulfilled by the Lead Contact, Ana Traven (ana.traven@monash.edu). All unique/stable reagents generated in this study are available from the Lead Contact with a completed Materials Transfer Agreement.

EXPERIMENTAL MODEL AND SUBJECT DETAILS

Candida strains and growth conditions

For standard growth, *C. albicans* strains were grown in YPD (1% yeast extract, 2% peptone, and 2% glucose, 80 μg/ml uridine with addition of 2% agar for plates) at 30°C with shaking at 200 rpm. For growth on different carbon sources, YP agar plus 2% lactic acid (lactate), 2% glycerol, or 2% ethanol were used. For analysis of sensitivities to various chemicals, ten-fold serial dilutions of overnight-grown cultures starting from an optical density (OD_{600nm}) of 0.5 were plated on control plates, or plates containing the compounds indicated in the Figure legends. Plates were incubated at 30°C for 2 or 3 days and then photographed. For hyphal growth, overnight-cultured strains were washed with PBS twice, diluted to OD_{600nm} 0.2 into pre-warmed RPMI 1640 pH 7.2 (buffered with 0.165 mol/L MOPS), and grown at 37°C with shaking at 200 rpm. Alternatively, overnight-grown cultures were diluted to obtain single colonies, and 100 μL were plated on the RPMI plates or Spider plates (1% mannitol, 1% nutrient broth and 0.2% K_2HPO_4, 2% agar). Incubation was at 37°C for 5 days.

For determining cell viability following CFW treatment, overnight-cultured strains were diluted to OD_{600nm} of 0.2 and grown to an OD_{600nm} of 0.8. These log-phase cells were then incubated in YPD with or without 20 or 30 ug/ml CFW for 15, 30, 60 and 120 min. At the indicated time points, cultures were serially diluted, plated on YPD agar plates, incubated for 3 days at 30°C and then colonies counted.

Mice

The Monash Animal Research Platform (MARP) provided mice (BALBc) for the virulence experiments in this study. The age of the mice was 6-8 weeks, and the sex was female. Maintenance and care conditions were as follows. Access to food and water was unrestricted (standard chow, Ridley, product code #102119-1040) and the light-dark cycle was 12 h. Before experiments, the adjustment period for the animals was 1 week in the animal facility. Animal experiments were approved by the Monash University Animal Ethics Committee (approval number MARP-2015-170).

METHOD DETAILS

Strain construction

The various *taf14* or *yaf9* mutants were generated from strain SN152 (*his1*$^-$ *leu2*$^-$ *arg4*$^-$). Homozygous *taf14*Δ/Δ (*HIS1*$^+$ *LEU2*$^+$ *ARG4*$^+$) and *yaf9*Δ/Δ (*HIS1*$^+$ *LEU2*$^+$ *ARG4*$^+$) were produced by stepwise deletion of *TAF14* or *YAF9* alleles utilizing the *C. dubliniensis HIS1* and *C. maltose LEU2* markers, followed by insertion of *C. dubliniensis ARG4* into the *LEU2* locus to produce a fully prototrophic strain (Noble et al., 2010; Noble and Johnson, 2005). The complemented strain *taf14*Δ/Δ+*TAF14* (1X) (*HIS1*$^+$ *LEU2*$^+$ *ARG4*$^+$) was engineered by introducing one copy of wild-type *TAF14* at the *LEU2* locus of *taf14*Δ/Δ (*HIS1*$^+$ *LEU2*$^+$ *arg4*$^-$) using the *C. dubliniensis ARG4* marker. The complemented strain *taf14*Δ/Δ+*TAF14* (2X) (*HIS1*$^+$ *LEU2*$^+$ *ARG4*$^+$) was constructed by introducing the second wild-type *TAF14* copy in the *taf14*Δ/Δ+*TAF14* (1X) strain at the endogenous *TAF14* locus just upstream of the *HIS1* disruption cassette. For this, the modified *NAT1* selectable marker was used (Shen et al., 2005). The

taf14W80A (*HIS1*$^+$ *LEU2*$^+$ *ARG4*$^+$) and corresponding complemented strain *taf14Δ/Δ+TAF14* (*HIS1*$^+$ *LEU2*$^+$ *ARG4*$^+$) were constructed in a similar manner as the *taf14Δ/Δ+TAF14* (2X) strain, with the difference that two copies of *TAF14*^{W80A} (from TGG to GCT) or wild-type *TAF14* cDNA (no intron) were introduced back into *taf14Δ/Δ* genome. Complemented *yaf9Δ/Δ+YAF9* (*HIS1*$^+$ *LEU2*$^+$ *ARG4*$^+$) was produced by integrating *YAF9* plus *C. dubliniensis ARG4* into the *yaf9Δ/Δ* strain at the *LEU2* locus. For re-integration of *TAF14* or *YAF9* wild-type and mutant genes in the respective mutant strains, the expression was driven by their endogenous promoter and terminator regions. Taf14-TAP (*HIS1*$^+$ *leu2*$^-$ *ARG4*$^+$) was constructed by introducing a TAP tag amplified from plasmids pFA-TAP-*HIS1* or pFA-TAP-*ARG4* by PCR at the C terminus of *TAF14* (Lavoie et al., 2008), in the parental strain SN152. Both alleles were tagged (one using the *HIS1* marker and the other using the *ARG4* marker). All transformants were confirmed by diagnostic PCR. The strain SN425 (*HIS1*$^+$ *LEU2*$^+$ *ARG4*$^+$), a prototrophic strain derived from SN152, was used as the wild-type reference. The chromatin mutant strains used in Figure 1D were from the Kuchler lab, and are described in the Key Resources Table.

Zymolyase Treatment

Zymolyase treatment was performed as described in Zavrel et al. (2012). Cells were grown to stationary phase, pelleted, washed, and then re-suspended in buffer (50 mM Tris-HCl, pH 7.5, 60 mM beta-mercaptoethanol in 1.5 mL cuvettes. The initial OD_{600nm} was ~1. Zyomolase was added to 2 U/ml (Zymolyase 100T, US Biological life sciences, Cat# Z1004). Given the propensity of cells to precipitate, the medium in the cuvette was vortexed before measuring absorbance. Absorbance (OD_{600nm}) was measured every 5 min for 1 h.

Microscopy

Cell images were taken using the EVOS FL AUTO Imaging System. For imaging cell morphology in Figure 3D, overnight cultures were harvested at 3000 rpm, washed with PBS, re-suspended and then sonicated for 10 s to separate cell clumps. Cells were then mixed with equal amount of mounting medium (10 μl) on microscopy slides, covered with coverslips and visualized by microscopy (100X magnification). For hyphal morphology in Figure 3G, overnight-grown cultures were diluted to OD_{600nm} = 0.2 in 20 mL RPMI media. After growth of 4.5 h at 37°C, cells were harvested at 3000 rpm for 5 min at room temperature, washed with PBS, re-suspended in 500 μL and sonicated for 10 s to separate clumps. Microscopy slides were made as described above, and imaged at 40X magnification. Hyphal length was measured using ImageJ 1.52a software. Images of colonies on filamentation on plates were captured using a stereo dissecting microscope (Olympus SZX 16).

RNA-seq analysis of gene expression

Wild-type and *taf14Δ/Δ* cells from a stationary overnight-grown culture were diluted to an initial OD_{600nm} of 0.2 in YPD media and grown to an OD_{600nm} of 0.8-1.0 at 30°C in a shaking incubator (200 rpm). These log-phase cultures of wild-type or mutant (20 ml) were centrifuged at 3000 rpm at 4°C for 5 min, washed with water and pelleted into screw tubes as -CFW or -crotonate samples. Another 20 mL of culture was incubated in YPD with 20 μg/ml of calcofluor white or 50 mM crotonate for an additional 2 hours at 30°C (200 rpm), and harvested as mentioned above, as +CFW or +crotonate samples. All cell pellets were immediately frozen in dry ice and stored at −80°C until further use.

Total RNA extraction from two independent biological replicates was done using the hot phenol method and the PAT-seq libraries were prepared as described previously (Koch et al., 2018; Tucey et al., 2018). PAT-seq libraries were sequenced with the Illumina Hiseq1500 platform with 100 base rapid chemistry according to the manufacturer's instructions. The raw sequencing data were processed by the Tail Tools pipeline (https://github.com/Monash-RNA-Systems-Biology-Laboratory/tail-tools) as described previously (Harrison et al., 2015). Data were aligned to the SC5314 assembly (plus AF167163 downloaded from NCBI). To test for differential expression, first genes with less than 50 reads in all samples tested were discarded (in other words, the genes needed to have 50 reads in at least one sample to be kept for analysis). Library sizes were estimated, and read counts were normalized and converted to RPM (reads per million) using the TMM method from the edgeR R package (Robinson and Oshlack, 2010). Read counts were log-transformed and weighted using the voom method (Ritchie et al., 2015). Significant differential expression was detected using the Fitnoise package (https://github.com/pfh/fitnoise). The analysis for the entire dataset can be accessed at http://rnasystems.erc.monash.edu/2019/verma_et-al/. The heatmap of changes in gene expression of differentially regulated genes were created using the R package gplots (Figures 4 and 7) (Warnes et al., 2019). The Venn diagram in Figure 4B shows the overlap of genes differentially expressed in CFW-treated WT and untreated *taf14Δ/Δ* mutant, with untreated WT as the baseline for comparison in both cases (FDR < 0.01; log2 of 1). The Venn diagram in Figure 7C shows the overlap between genes differentially expressed by CFW or crotonate (FDR < 0.01, log2 of 1). The GO term analysis of biological process and component represented in differentially regulated genes was performed using tools at the *Candida* Genome Database (Data S2).

To check for any evidence of gross chromosomal changes in the *taf14Δ/Δ* strain (Figure S4), the RNA-seq data were analyzed by mapping to the *C. albicans* reference genome using the STAR aligner and quantified using featureCounts. Then the log2 fold change was calculated for each gene of *taf14Δ/Δ* separately to a "baseline," where the baseline was the average of the two WT untreated samples. Genes with a low expression of less than one count-per-million were filtered out. Then a moving average of log2-fold-change was calculated along each chromosome by computing the average of the log2-fold-change of every gene in a 10kb window. This moving average of log2-fold-change was then examined for evidence of an aneuploidy event.

qPCR analysis of gene expression

Overnight-grown cultures were diluted to an OD_{600nm} of 0.2 and grown in YPD with uridine media at 30°C to log phase (approximately 2 generations). Total RNA was isolated by the hot phenol method, then 1 μg of DNase I - treated total RNA was reverse-transcribed to cDNA using Superscript III (Invitrogen). qPCR of gene expression was performed with the FastStart Universal SYBR green master mix according to the manufacturer's instructions on a LightCycler 480 (Roche). Data were analyzed with the LinReg software (Ruijter et al., 2009). Normalization was performed using the expression levels of the *RDN5* gene. The number of biological repeats is stated in the Figure legends, and each biological repeat was assayed in two technical repeats. For data analysis, the technical repeats were averaged to obtain the expression value for the biological repeat. Statistical analysis was performed on the normalized expression values (Figure S2B) or log2-transformed normalized expression values (Figure 5E) for the biological repeats. Sequences for all qPCR primers used in this study are listed in Table S1 and references are Tucey et al. (2016); Uwamahoro et al. (2014), and Verma-Gaur et al.(2015).

Chromatin immunoprecipitation (ChIP)

ChIP assays were performed as described previously (Hernday et al., 2010). Cells were grown to an OD_{600nm} of ~0.9 −1.0 followed by treatment with or without calcofluor white (20 μg/ml) for 30 min, and then fixed in growth media with 1% formaldehyde for 10 min, quenched with 125 mM glycine and washed with PBS. Cell lysis was performed in buffer (50 mM HEPES/KOH (pH 7.5), 140 mM NaCl, 1 mM EDTA, 1% Triton X-100, and 0.1% sodium deoxycholate) including 1X complete protease inhibitor cocktail (Roche) and 10 mM sodium butyrate using glass beads. Chromatin was sheared to ~300 bp with 12 rounds of sonication (30 s on, 30 s off) on a Bioruptor (Diagenode). Input volume of 10% was set aside. The immunoprecipitation (IP) was performed by incubating overnight at 4°C with 5 μg of the H3K9cr antibody. The next day, 50 μl of Protein A dynabeads (Invitrogen) were added to the IP samples and incubated for 2 hours at 4°C. A magnetic stand was used to separate beads from extract. Washing of IP samples was as follows: 2 times with 1 mL cell lysis buffer, 2 times with 1 mL cell lysis buffer with 500 mM final NaCl, 2 times with 1 mL of LiCl buffer (10 mM Tris pH 8, 1 mM EDTA, 0.25 M LiCl, 0.5% NP-40, 0.5% sodium deoxycholate) and 2 times with 1 mL of TE buffer (10 mM Tris pH 8, 1 mM EDTA). Chromatin was eluted with elution buffer (50 mM Tris pH 8, 10 mM EDTA 1% SDS), and de-crosslinked overnight at 65°C, followed by treatment with Proteinase K and RNase. Following this, a purification by phenol chloroform and ethanol precipitation was performed. A dilution of 1:20 was made for input and IP ChIP samples and qPCR was performed by Fast-Start Sybr Green Master mix using primers described in Table S1.

Murine infection model

Mice were systemically infected by injection into the tail vein with $3x10^5$ CFUs of *C. albicans* and kidney load determined as described before (Tucey et al., 2018). The animals were checked daily for clinical signs of infection including weight loss (20% of initial body weight), followed by humane euthanasia when they reached experimental end points as per the approved protocol.

Western blot analysis

All antibodies used in this study are listed in KEY RESOURSES TABLE. For detecting the levels of the H3K9cr and H3K9ac marks, samples were prepared as follows. Overnight-grown cultures were diluted to an OD_{600nm} of 0.2 and grown in 10 mL YPD with uridine media at 30°C to log phase (Figures 1A and 1D). In Figures 1B, 1C, and 7A, log phase cultures were treated with sodium crotonate at the indicated doses (prepared from crotonic acid by adjusting pH to 7.4 using sodium hydroxide), sodium butyrate, TSA (Trichostatin A) and calcofluor white (CFW) for the indicated incubation times. In Figure 1E, log phase YPD-grown cells were pelleted, washed twice by PBS, resuspended in 10 mL of YP, YP with 0.2% glucose, 2% glucose, 2% lactate or 2% ethanol supplemented with uridine and grown at 30°C for 3 h before harvesting for protein extraction. For detecting phosphorylated Mkc1 and Cek1 (Figure 3C), 100 mL of log-phase YPD-grown cells were treated with 20 μg/ml CFW, and 10 mL harvested at 0, 15, 30, 60 and 120 min. For detecting Taf14 (Figure S5), samples were grown to log phase as described above. All cell pellets were frozen in dry ice immediately and stored at −20°C.

Whole cell protein extracts were made by adding 100 μL of glass beads, and 100 μL 20% TCA (trichloroacetic acid) to cell pellets in 1.5 mL screw cap tubes, and the tubes frozen on dry ice until TCA froze. The tubes were warmed by vortexing for 2 min and supernatant transferred to a new 1.5 mL centrifuge tube. The glass beads in the old tubes were washed with 500 μL of 10% TCA, and supernatants added back to the tubes containing previous supernatants. The pooled supernatants were centrifuged at 14000 rpm for 5 min and precipitated proteins were washed with 1 mL ice cold acetone, re-suspended in high pH Laemmli Buffer (0.0625M Tris pH 8.8, 2% SDS, 10% glycercol, 5% mercaptoethanol, 0.01% saturated bromophenol blue) and boiled at 100°C for 5 min. Boiled samples were loaded on a 15% (Figures 1 and 7A) or 12% (Figures 3C and S5) SDS-PAGE and transferred to PVDF membrane. Membranes were blocked with SuperBlock (for H3 antibody), 5% BSA in TBS-T (TBS with 0.1% Tween) for Phospho-p44/42 MAPK (Erk1/2) (Thr202/Tyr204) antibody, or 5% milk in TBS-T for other primary antibodies for 1 hour and then incubated with primary antibodies in respective blocking buffers overnight at 4°C with gently shaking. For the anti-actin antibody, incubation was for 1 hour at room temperature. Following this, membranes were washed three times for 5 min with TBS-T. HRP conjugated secondary antibodies were used at 1:20,000 in 5% milk powder in TBS-T for 1 hour at room temperature, and washed three times for 5 min in TBS-T. For detection of histone modifications, membranes were visualized using Amersham ECL western blotting detection reagent. For detection of Phospho-p44/42 MAPK (Erk1/2) (Thr202/Tyr204), Taf14 and actin membranes were visualized using Clarity Western ECL substrate, and

exposed to FUJI medical X-ray film. Ponceau-stained membranes or actin were used as loading reference, as indicated in the Figure legends. In Figure S6, the actin antibody was used as the loading control. The membrane used to detect Taf14 level was stripped with 0.5 M sodium hydroxide for 10 min, followed by washing with water, TBS-T and water for 5 min each time. Following stripping, the membrane was dried and then used for detection of the levels of actin. Quantification of western blots was done with ImageQuant 1D version 7.0. Background signals were subtracted using the local median method performed by the software.

Dot blot analysis

In Figure S1A, the testing of the specificity of the H3K9cr antibody was performed using dot blot analysis as previously described (Andrews et al., 2016b). Peptides of unmodified H3 (1-19), H3K9cr, H3K9ac or H3K9bu peptides (0.06–1.5 μg) were spotted onto a nitrocellulose membrane and then a 1:2000 dilution of H3K9cr or H3K9ac antibody in 5% milk powder in TBS-T was used to probe the membrane. A 1:20,000 dilution of HRP-conjugated secondary antibody and the Amersham ECL western blotting detection reagent were used for detection.

Binding assays of Taf14 with H3K9cr and H3K9ac peptides

Binding assays were done using cell extract from log phase grown cultures of Taf14 WT and *taf14*W80A strains. Cell extracts were prepared in buffer (50 mM Tris-HCl (pH 8.0) 150mM NaCl, 2mM MgCl2, 0.1% NP40) including 1X complete protease inhibitor cocktail (Roche). Peptide pull down assays were performed using 1 nmol biotinylated H3 (1-19), H3K9cr or H3K9ac peptides immobilized on streptavidin beads by incubating overnight with WT or *taf14*W80A cell extract. The beads were washed with buffer (50 mM Tris-HCl (pH 8.0) 500mM NaCl, 2mM MgCl2, 0.1% NP40 + 1X complete protease inhibitor cocktail). Bound proteins were detected by western blot analysis using the anti-Taf14 antibody as described above.

Bioinformatic analysis

Fungal protein sequences were downloaded from the Ensembl genomes database (ftp://ftp.ensemblgenomes.org/pub/fungi/release-31/fasta/, on May 2016) and the YEATS proteins were annotated using HMMER (software version of 3.1) and NCBI BLAST. After removing obsolete sequences (33 isolates of 16 species) from the latest Ensembl genomes database (April 2019, http://ensemblgenomes.org/), and manually finding incomplete data (3 isolates of 3 species), the final fungal protein sequence dataset contained 553 isolates of 319 fungal species and was subsequently used for the analysis. To build the prediction model, 370 known fungal YEATS domains were retrieved from the Pfam database (http://pfam.xfam.org/; as of May 2016; Data S1) and used to construct the Hidden Markov Model (HMM) profile according to the HMMER manufactures' instructions. The prediction model HMM was utilized to search for putative YEATS proteins against the fungal proteomes. Software HMMER 3.1 provided the statistical significance E-values for these putative YEATS hits. To reduce false-positive YEATS proteins, the predicted YEATS proteins were further validated by NCBI BLAST. As a result, YEATS proteins with E-value $\leq$ 2.20E-04 were kept. Finally, all positive YEATS proteins were confirmed by both HMMER and BLAST. Next, these proteins were annotated with gene IDs referring to the Ensembl database (http://ensemblgenomes.org/). NCBI database was used to check if there is updated information about these isolates and species. The information in Data S1 was updated as of April 2019 according to the NCBI and Ensembl databases. The numbers of YEATS proteins for each species were counted as follows: (1) for the species with one isolate, the YEATS protein number of the isolate was chosen as the YEATS protein number for the species (e.g., *Acremonium chrysogenum*); (2) for the species with two or more isolates (e.g., *Trichoderma reesei* and *Saccharomyces cerevisiae*), the higher YEATS protein number between the isolates was chosen as the YEATS protein number for the species In *C. albicans*, 23 of 24 isolates have two YEATS proteins, while only one has three YEATS proteins. However, two of the three proteins have the same protein sequences and are likely to be caused by gene duplication. *C. albicans* was therefore considered to have two YEATS proteins. In *R. solani*, three isolates have one YEATS protein, while two have two YEATS proteins. *R. solani* was considered to have two YEATS proteins. Next, to examine the sequence homology between the YEATS proteins in the selected fungal species and the YEATS family members from *S. cerevisiae* as the standard (Yaf9, Taf14 and Sas5), pairwise sequence alignment was constructed with BLAST. The YEATS proteins with highest max scores aligning to *Sc*Yaf9, *Sc*Taf14 and *Sc*Sas5 are shown in Data S1, and selected species are shown in Figure 2B.

QUANTIFICATION AND STATISTICAL ANALYSIS

GraphPad Prism 7 was used for all statistical analyses. Details of statistical method used are described in the figure legends. Statistical analysis of mice survival curves was done using the Mantel-Cox test. ChIP-qPCR data were analyzed using Welch's t test. For statistical analyses of multiple groups except qPCR data in Figure 5E, one-way ANOVA was used followed by Tukey's multiple comparisons. In the case of Figure 5E, two-way ANOVA was used followed by Tukey's multiple comparisons. *P values* < 0.05, *; *P values* < 0.01, **; *P values* < 0.005, ***; *P values* < 0.001, ****.

DATA AND CODE AVAILABILITY

The RNA-seq dataset has been deposited in GEO: GSE128279 and GSE141229.